N71-26284 56

~~NASA CR-72677~~

Should be CR-72877

THRUST VECTORING SYSTEMS

PART I – 5 cm SYSTEMS

By

H. J. KING, C. R. COLLETT, and D. E. SCHNELKER

CONTRACT NAS 3-14058

Prepared for

NATIONAL AERONAUTICS AND SPACE ADMINISTRATION

HUGHES RESEARCH LABORATORIES

A DIVISION OF HUGHES AIRCRAFT COMPANY

3011 Malibu Canyon Road
Malibu, California 90265

5 cm THRUST VECTORING SYSTEM

by

H.J. King, C.R. Collett, and D.E. Schnelker

CONTRACT NAS 3-14058

FINAL REPORT

Prepared for

NATIONAL AERONAUTICS AND SPACE ADMINISTRATION

HUGHES RESEARCH LABORATORIES
a division of hughes aircraft company
3011 Malibu Canyon Road
Malibu, California 90265

Requests for copies of this report should be referred to

National Aeronautics and Space Administration
Scientific and Technical Information Facility
P.O. Box 33
College Park, Md. 20740

TABLE OF CONTENTS

ABSTRACT

Experimental data were taken with three different ion extraction systems (namely, the dual grid electrostatic, movable screen electrode, and vectorable discharge chamber systems), demonstrating that each is capable of vectoring the beam from a 5 cm thruster to ±10 degrees or more. The electrostatic system was chosen for a 100 hour endurance test over the latter two on the basis of speed of response and the absence of any moving parts. The performance of the electrostatic and movable screen systems is compared with that predicted on the basis of analytical models of each derived from a computer simulation of the ion trajectories of a single aperture. A table, comparing the merits of the various systems based on a wide range of criteria, is provided.

LIST OF ILLUSTRATIONS

LIST OF TABLES

SECTION I

SUMMARY

A number of techniques for controlling the direction of thrust from a mercury bombardment ion thruster were evaluated, the most promising were fabricated, and their performance experimentally documented and compared with that predicted from analytical models. The basic goal was to design an electrode system for a 5 cm thruster that would provide up to ten degree deflection of the thrust vector at all azimuths. The final selection was made from three systems — electrostatic dual grid, movable screen electrode, and vectorable discharge chamber. Functional hardware, representative of each of these systems, was fabricated and tested in a specially designed facility which was instrumented with a rake of movable Faraday cups to monitor the beam intensity over a plane normal to the thruster axis. This information was then processed by computer to provide contour plots of the beam intensity and the location of the thrust axis.

While all three systems meet the design specifications, the electrostatic system was considered the most promising on the basis of speed of response and the absence of any moving parts. It was subjected to a 100 hour endurance test during which time the beam was vectored to approximately ±10 degrees in each of two orthogonal axes. No degradation in vectoring capability was observed during the test period, and only slight erosion was evident on the downstream edges of the electrodes near the center of the beam following the test. The performance of the 5 cm thruster when operating with the dual grid electrostatic, movable screen and single grid glass coated nondeflecting optics systems is presented in the following table.

The conventional dual grid system in which the screen could be translated relative to the accelerator electrode is an acceptable alternative to the dual grid electrostatic design. While such a system is inherently slower than the electrostatic system because of the thermomechanical actuators, it was possible to vector the ion beam more than 20 degrees with slight interception at the accelerator. A particular advantage of the movable screen electrode is that it is equally applicable to thrusters of larger size, while the complexity of the mechanical design for electrostatic systems increases rapidly with thruster diameter.

A tabular comparison of the three deflection systems, based on 14 characteristics ranging from performance, to cost, to reliability, is included in a later section of this report.

SUMMARY OF 5 CM THRUSTER PERFORMANCE WITH THREE OPTICS SYSTEMS

Parameter	OPTICS SYSTEM		
	Dual Grid Electrostatic Deflection	Movable Screen Electrode Deflection	Single Grid Glass Coated Nondeflection
I_{beam}, mA	30	25	36
V_{beam}, V	1200	1000	600
Specific Impulse, sec	2240	2160	1670
Thrust, mlb	0.48	0.36	0.44
eV/ion	528	643	268
η^*_m discharge, %	64.5	68.2	68
$\eta^*_{electrical}$, %	48.2	39.0	41.3

*These efficiencies do not include the electrical power or mass flowrate of the neutralizer.

SECTION II

INTRODUCTION

Significant system simplifications can be achieved if the beam from an ion thruster can be vectored about the nominal thrust axis. For instance, the attitude control function as well as station keeping of a satellite can be accomplished by controlling the direction of the thrust from the millipound thruster necessary for station keeping alone. With primary propulsion systems, which use an array of much larger thruster modules, thrust vectoring may be used to accurately align the thrust vector and the vehicle center of mass to compensate for misalignments caused by failure of a thruster module, structural changes, or changes in power level.

While thrust vectoring had been achieved with various cesium ion thrusters, no reports describing the successful vectoring of the beam from a mercury bombardment thruster were available at the beginning of this contract.

In order to assure that no promising techniques for thrust vectoring were overlooked, the program, as defined in the Statement of Work, began with a very broad survey of thrust vectoring techniques and then narrowed the field of interest in successive stages to the point where a single system was endurance tested for 100 hours. A first selection was made from the list of those designs considered conceptually possible on the basis of the criteria listed in Table I. Preliminary designs for several systems were submitted to NASA, and four were selected for final design, fabrication, test, and delivery for further verification of their performance at NASA LeRC.

The special reports discussing the comparisons made at each level of selection plus the experimental data generated during the testing phase of the program (which has been subsequently verified at LeRC) should serve as a sound basis for the development of future systems for all sizes and types of bombardment thrusters. In particular, two systems (one electrical and one mechanical) were found to meet or exceed all specifications listed in the contract statement of work.

TABLE I

THRUST VECTORING TECHNIQUE CRITERIA

Criterion	Description and Comments
Deflection Angle	The maximum angle through which thrust vector must be deflected • may be discrete or continuous • may be a function of lifetime requirement
Deflection Azimuth	The azimuth about the main thrust axis over which the ion beam must be deflected • may be single axis • may be two axis (orthogonal) • may be 2π sr
Response Time	A measure of the speed at which the ion beam must be positioned
Pointing Accuracy	The absolute accuracy and stability with which the thrust vector can be positioned
Lifetime	The effect of ion beam deflection on thruster lifetime • may be a function of maximum deflection angle
Thruster Performance	The effect on thruster performance
Adaptability	The applicability of a given technique to various size thrusters (e.g., 5 cm to 30 cm)
Tested Concept	The extent to which the concept has been tested — thus minimizing design uncertainties
Development Time & Cost	Compatibility of time and cost resources available to the proposed program
Weight	The weight penalty associated with the incorporation of a thrust vectoring system
Power	The power (both steady-state and peak) required to vector the ion beam
Reliability	The confidence that the system will survive launch and function for the duration of the mission
PC&C Requirement	The complexity of the power conditioning and control system required to operate the thrust vectoring system
Thruster Design	The effect on basic design of the thruster • some techniques may require discharge chamber and/or neutralizer redesign • should be minimized (to minimize risk)

T144

SECTION III

EVALUATION OF THRUST VECTORING CONCEPTS

The first major tasks under the program reported here were to list the various possible thrust vectoring concepts in a manageable form and to provide a set of criteria against which the relative merits of each system could be judged. These criteria are listed and defined in Table I.

The systems were classified first as to the type of ion optical element used and second as to over-all array geometry. The number of possibilities discussed in the first special report[1] totaled nearly thirty. Of these, four appeared to be the most promising and were chosen for experimental evaluation. These were

- Dual grid system with electrostatic deflection
- Single (insulated) grid system with electrostatic deflection
- Dual grid system with deflection by controlled aperture misalignment
- Vectorable discharge chamber.

The reader is referred to the above referenced report[1] and to the subsequent design report[2] for a complete listing of the systems which were analyzed and the reasons for their rejection. The systems listed above are discussed in the following text.

A. ELECTROSTATIC DEFLECTION SYSTEM — DUAL AND SINGLE GRID

1. System Analysis

The technique of electrostatically deflecting the beam from an ion thruster has been discussed in detail by Anderson[3] and Worlock.[4] Basically, it consists of imposing a transverse electric field across the ion beam in the region of the negative accelerator electrode prior to neutralization. Such a technique was first applied to cesium contact thrusters of both single circular aperture and linear strip configurations. Extension of this concept to bombardment thrusters whose ion extraction system consists of a two-dimensional array of circular apertures is made mechanically difficult because each aperture in the accelerator must contain four deflection plates electrically isolated from each other. Analysis of such a system is equally difficult because of the asymmetries introduced in the shape of the electric field in the circular aperture by the deflection voltage, and the fact that the plasma surface from which the ions are emitted will move to coincide with one of these equipotentials. Because these two effects are interdependent, an iterative procedure is required for an exact solution. This fact, coupled with the further complication that the solution of the ion trajectories in the presence of their own space charge also requires an iterative solution, forces an analysis that is far beyond our current computational capabilities.

As a result of the inability to solve the exact problem specified above, a compilation of results generated using both digital and analog computer models as well as closed analytical expressions were used to estimate the deflection sensitivity and beam handling capability of the system. These results abstracted from a second special report comparing the various systems[2] are as follows.

- The tangent of the deflection angle is given by the equation

$$\tan\theta = k_{eff}\left(\frac{V_d}{V_{avg}}\right)\left(\frac{L}{D}\right) \qquad (1)$$

where

θ = deflection angle (degrees)

L = length of deflection plates (i.e., the thickness of the accelerator electrode (cm))

D = diameter of the aperture in the accelerator electrode (cm)

V_d = total deflection voltage applied across the accelerator aperture (V)

V_{avg} = average voltage through which the ions have been accelerated at the accelerator (i.e., $V_{beam} + |V_{accel}|$ (V)

k_{eff} = deflection sensitivity.

While the limiting value of k_{eff} is 0.5 as L approaches infinity,[5] it was estimated that because of the large end effects, the actual value could be as high as three for the short deflection regions employed here.

- The average deflection angle was expected to be a weak function of the plasma boundary except for very close accelerator screen electrode spacings.
- The ratio L/D is important in determining both the deflection sensitivity and the maximum current handling capability of the ion extraction system. This is illustrated in Fig. 1, where the beam diameter is plotted versus the normalized deflection length for deflection angles of 10 to 16 degrees. The figure shows that to prevent interception ($\theta < \theta_{crit}$), it is necessary to reduce the entrance beam size as the deflection system is made longer. Thus, there is a tradeoff between deflection length (which affects deflection sensitivity) and entrance beam diameter. For example, for a 10 degree beam deflection, as the normalized deflection length (defined as the ratio of the length of the deflecting electrodes to their

spacing or diameter) varies from 0.25 to 1.0, the maximum normalized beam diameter decreases from 0.91 to 0.65. The two points shown in Fig. 1 are extrapolated from digital computer trajectory calculations.

- The beam size at the point at which it enters the accelerator aperture is governed by the extraction geometry. Figure 2 shows the plot of perveance per hole versus the normalized beam diameter for two different extraction geometries. As the plasma sheath recedes into the screen hole, the perveance per hole and the beam diameter defined by the outer edge trajectory both decrease in the manner shown. Presumably, this curve would start rising again when direct crossovers start to occur.

The above analysis suggested an ion extraction system with the following characteristics for the 5 cm thruster:

Number of apertures	97
Beam current	30 mA
Beam voltage (A/D = 2.0)	1.1 kV
Thrust	0.46 mlb
L/D of accel aperture	0.74

Figure 3 illustrates both a dual grid aperture and a single insulated electrode aperture which satisfy the above criteria for a 5 cm thruster.

2. Design and Fabrication

After considering a number of alternatives, the only practical design which satisfied the electrical constraints was an "eggcrate" structure assembled from interlocking strip electrodes as is illustrated in Fig. 4. Careful inspection of this figure reveals that each aperture is bounded by the necessary four electrically independent electrodes and that the individual strips may be interconnected at the periphery of the

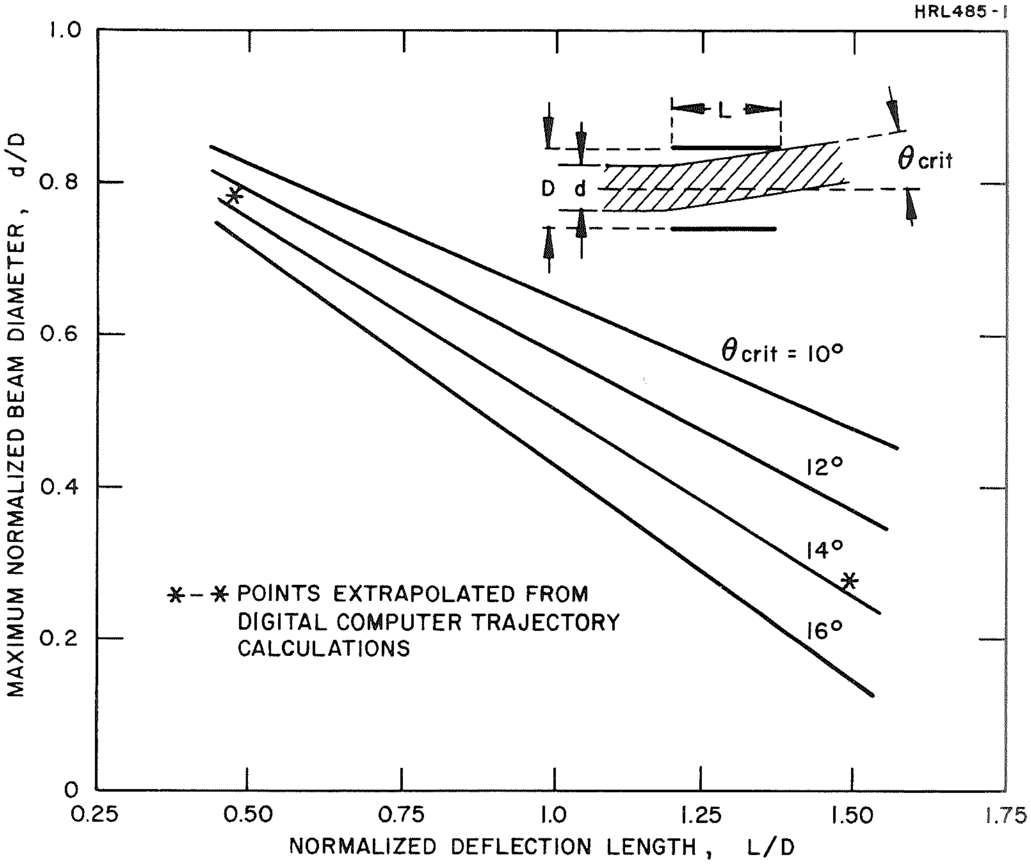

Fig. 1. Maximum Beam Diameter as a Function of Normalized Deflection Length.

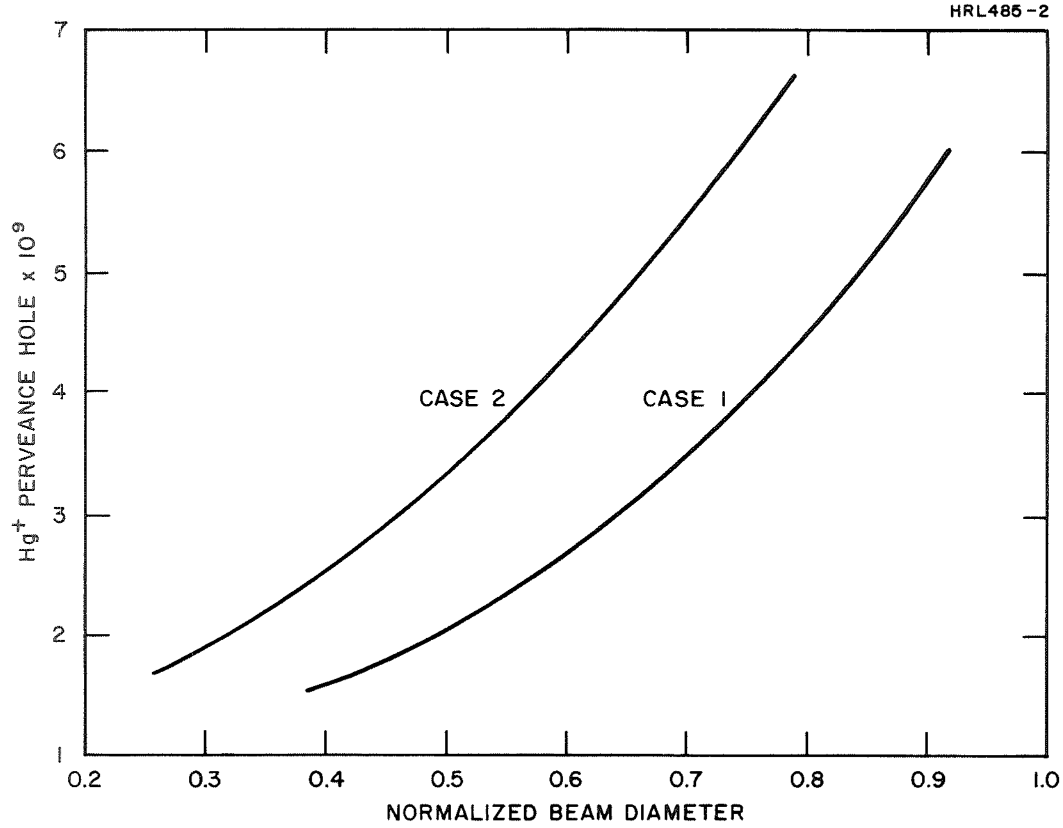

Fig. 2. Perveance per Hole versus Normalized Beam Diameter. (L/D = 0.42 for Cases 1 and 2, Accel to Screen Spacing = 0.229 cm for Case 1 and 0.178 cm for Case 2.)

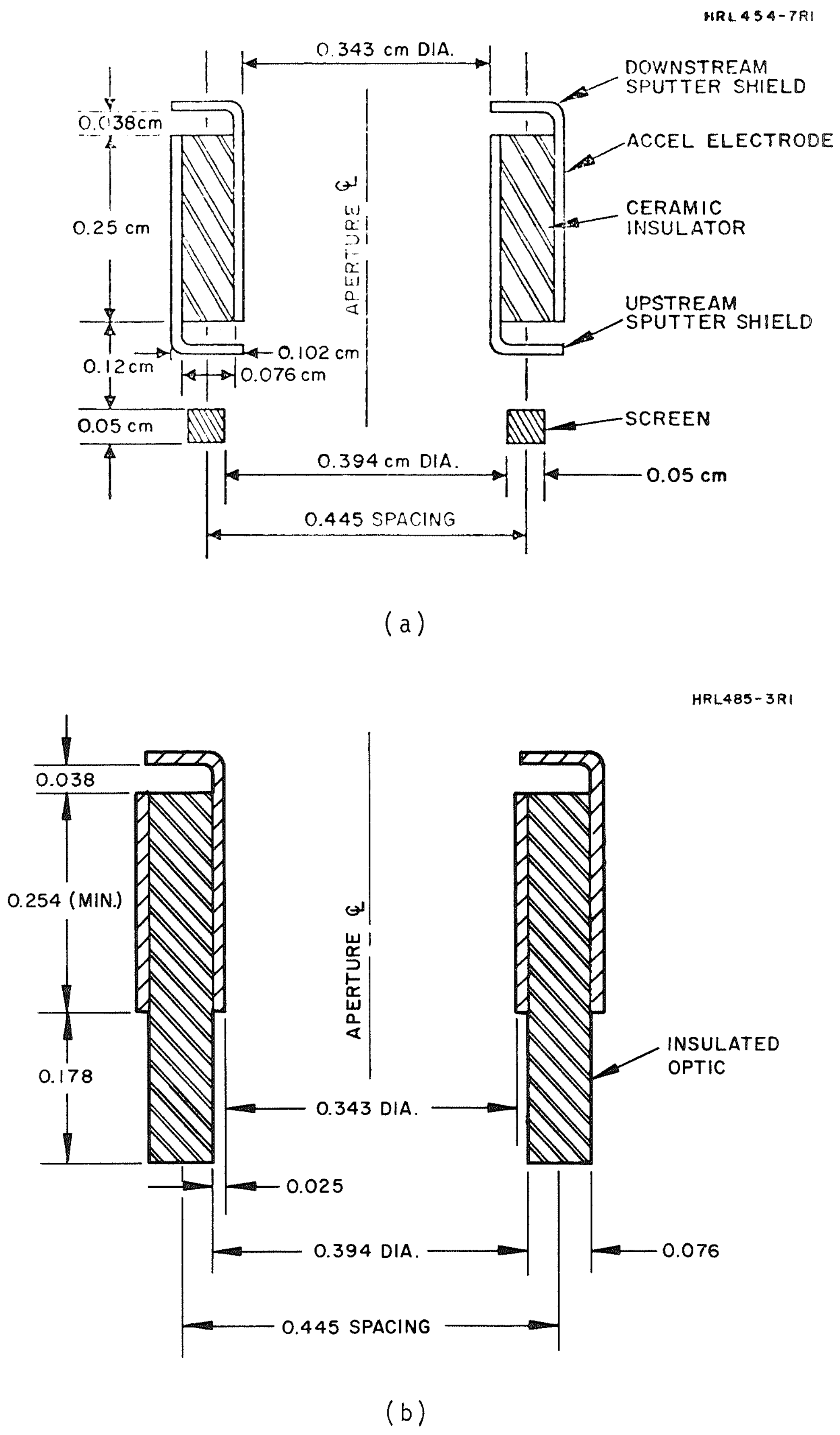

Fig. 3. Electrode Aperture Designs. (a) Dual Grid. (b) Single Grid.

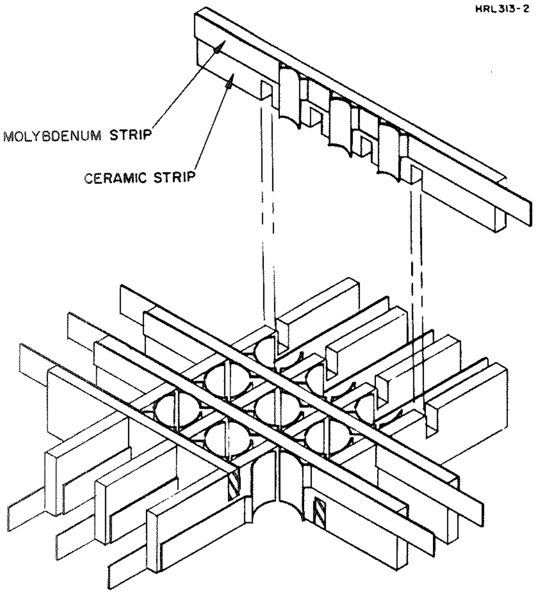

Fig. 4.
Basic Interlocking Egg-crate Electrode Design Structure.

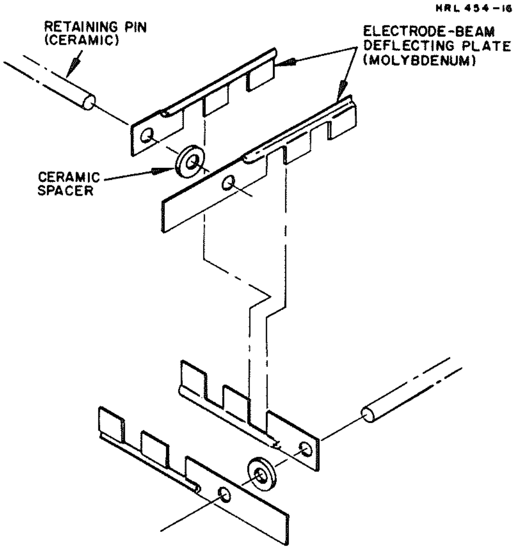

Fig. 5.
Vectorable Dual Grid Extraction System.

electrode. Figures 5 and 6 illustrate the application of this concept to both the accelerator of a dual grid system and to a single insulated grid structure where the edge of the insulating material between the strips serves as the region of plasma attachment.

A considerable effort was expended to perfect the brazing techniques used to fabricate these parts and to form the electrode strips so as to maintain the required tolerances. A number of design modifications were implemented in order to improve the sputter shielding of the insulator material between the electrodes to prevent interelectrode shorting. While the fabrication and assembly procedures were readily solved, no satisfactory sputter shield design was found. As a result, the initial design (for the dual grid system) was modified to eliminate the ceramic strips between the electrodes entirely and to suspend the electrodes from the end supports only, as shown in Fig. 5. This modification resulted in a simpler system which was both cheaper and faster to assemble and which could be designed with a smaller L value, thus permitting a greater deflection angle before direct interception occurs. A system of this design was ultimately tested for 100 hours (see Section VII). A recent design concept has been evolved to permit each electrode to be individually tensioned, thus improving stability under thermal loading.

Unfortunately, because the interelectrode ceramic is required in the single grid system to anchor the plasma surface, it could not be eliminated there to provide similar improvements to the dual grid system. This was a principal reason for the ultimate rejection of the single grid electrostatic system.

Representative hardware of each of the above designs is shown in Figs. 7 and 8.

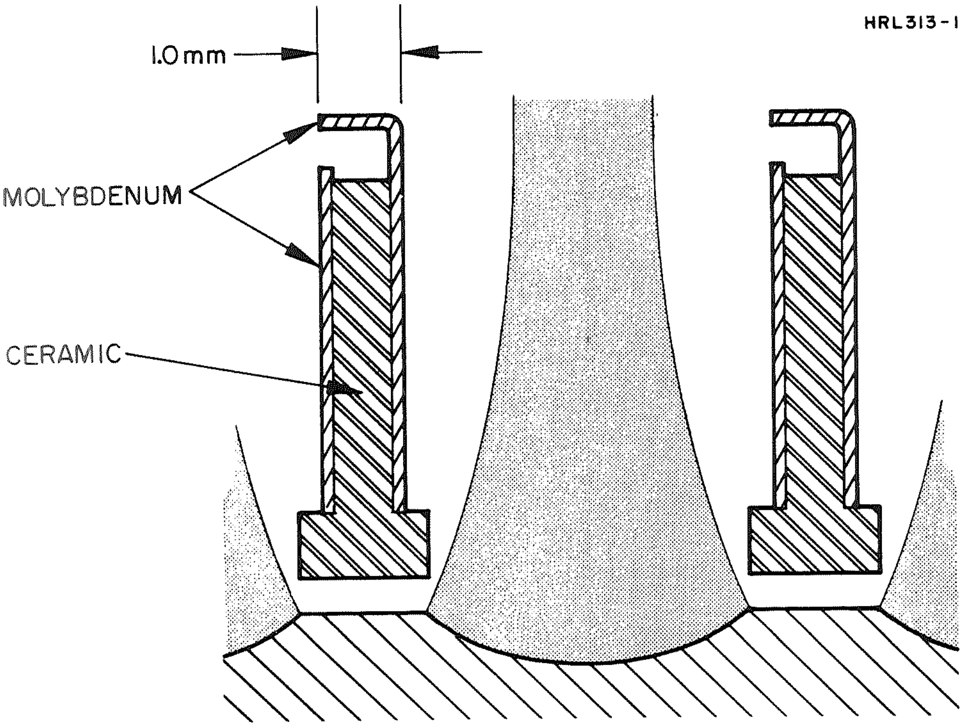

(a) Single Element.

Fig. 6. Vectorable Accelerator Single Electrode with Interelectrode Ceramic Spacers.

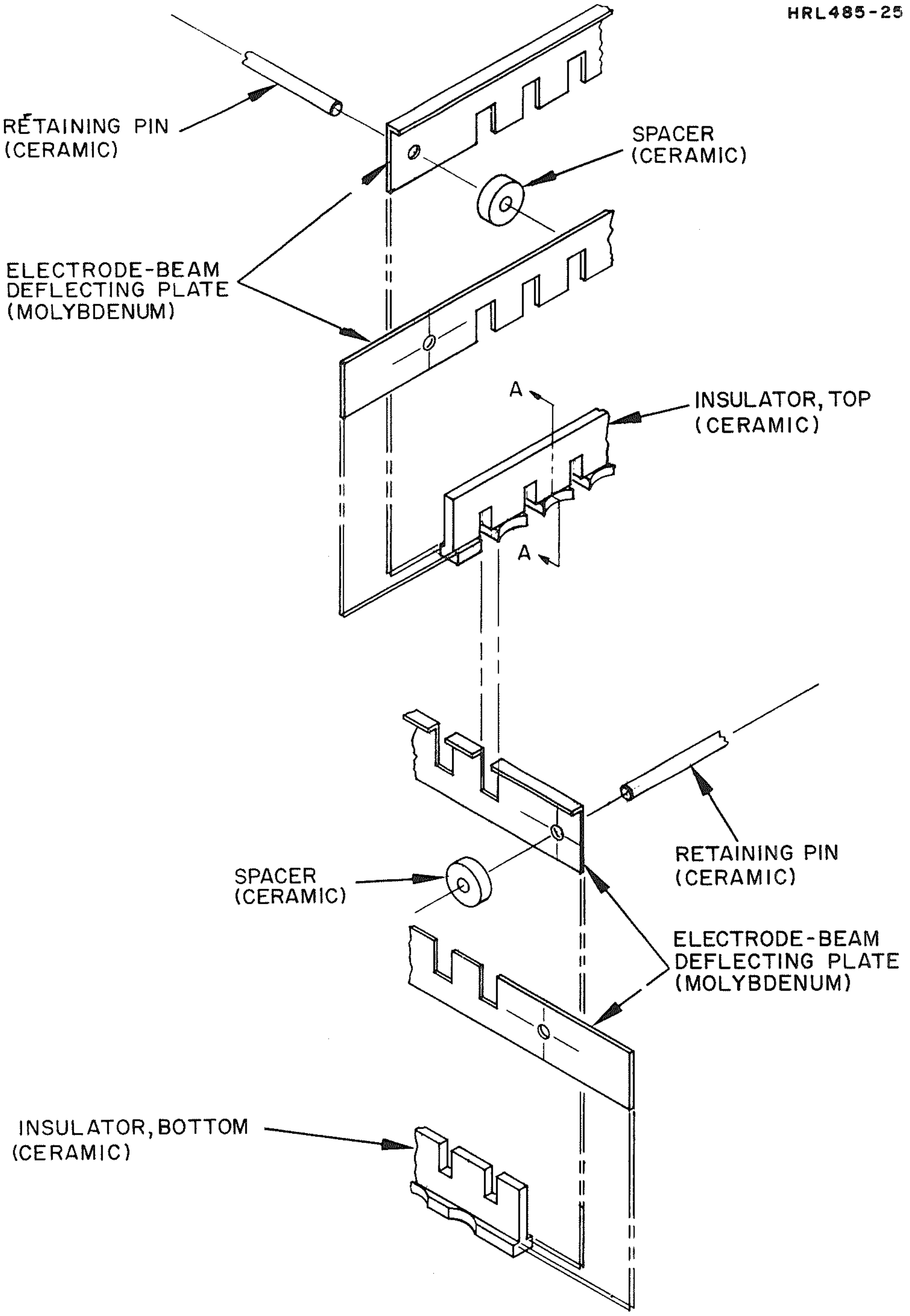

Fig. 6(b). Exploded View of Single Electrode Assembly.

M 7678

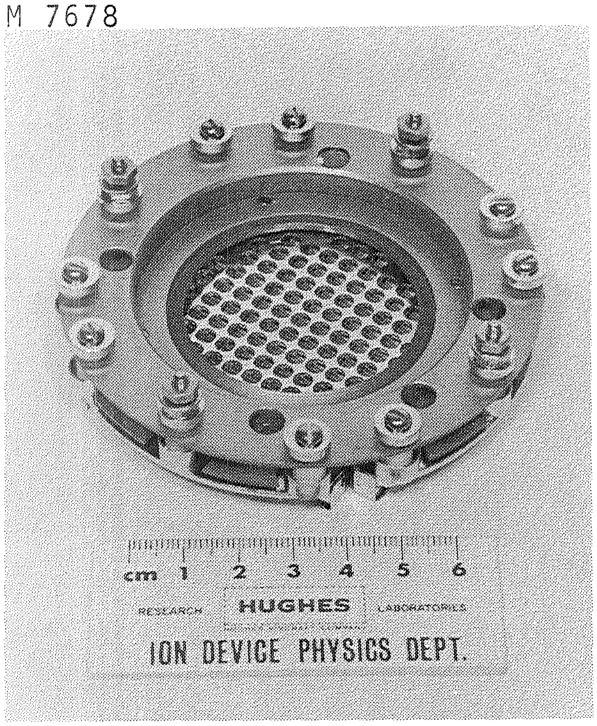

Fig. 7(a).
Electrostatic Dual Grid — Upstream Side.

M 7677

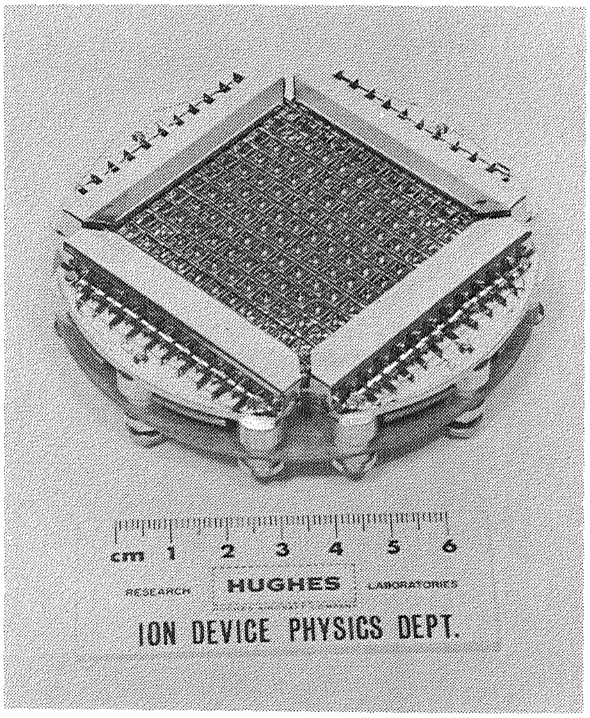

Fig. 7(b).
Electrostatic Dual Grid — Downstream Side.

M 7586

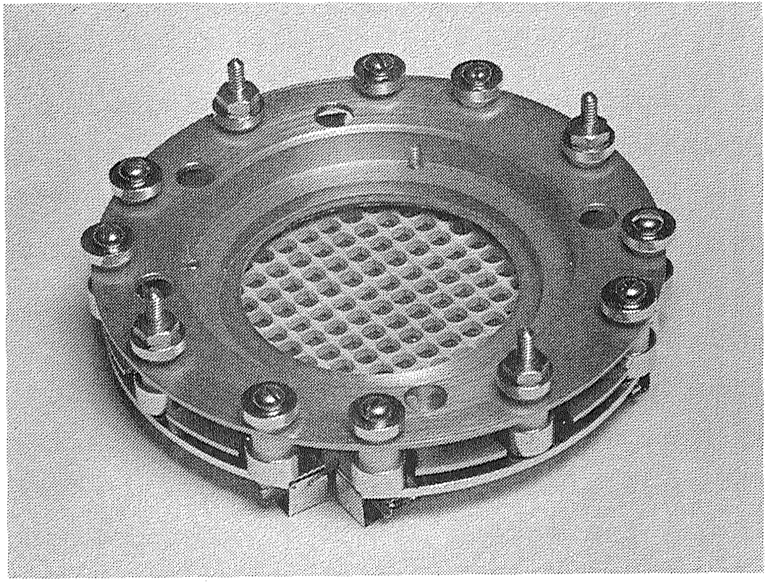

(a) Upstream Side.

M 7587

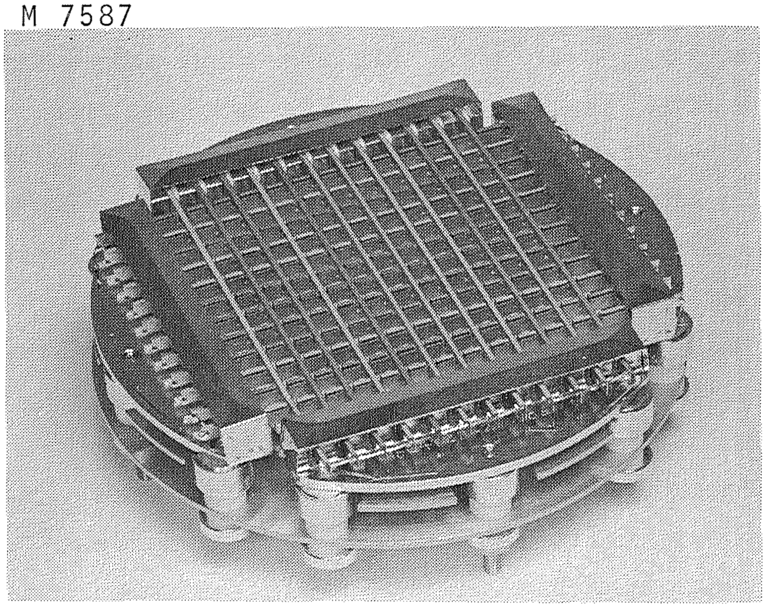

(b) Downstream Side.

Fig. 8. Photographs of Electrostatically Vectorable Single Grid Extraction System.

B. MOVABLE SCREEN DEFLECTION SYSTEM

It is intuitively apparent that a misalignment between the apertures in the screen electrode and the accelerator electrode in a conventional dual grid ion extraction system will produce a net deflection of the average ion trajectory. HRL has recently completed an extensive digital computer study of this effect as one part of an investigation of thrust vector misalignment and thrust stability for prime propulsion systems.[6] These studies quantitatively defined the trajectories of the ions as a function of the transverse motion between the screen and accel electrodes. Two geometries were studied with nominal transverse displacements of 5% and 10% of the accel hole diameter. Digital computer calculations of the self-consistent ion trajectories for these cases (calculated assuming planar symmetry) are shown in Figs. 9 and 10. Note that for the high perveance case the peripheral ions just intercept the accelerator. Thus, the nominal 8 degree deflection is a practical maximum to be expected with an unoptimized system. Figure 10 shows the same geometry operating at a lower arrival rate, where the more concave sheath produces a smaller beam diameter in the accelerator electrode plane. In this case, no accelerator electrode interception occurs. Linear extrapolation of these data indicates that direct interception of the crossover trajectories will begin at approximately double the deflection shown or at approximately 18 degrees. Analysis of the trajectories shown in the above figures resulted in the data plotted in Fig. 11, which shows that over the range studied, the mean angular displacement of the ion trajectories is a linear function of the accel electrode displacement. This figure also shows the mean angular displacement is nearly independent of the beam current with a deflection of 8.4 degrees for a displacement of 10% of the accel hole diameter.

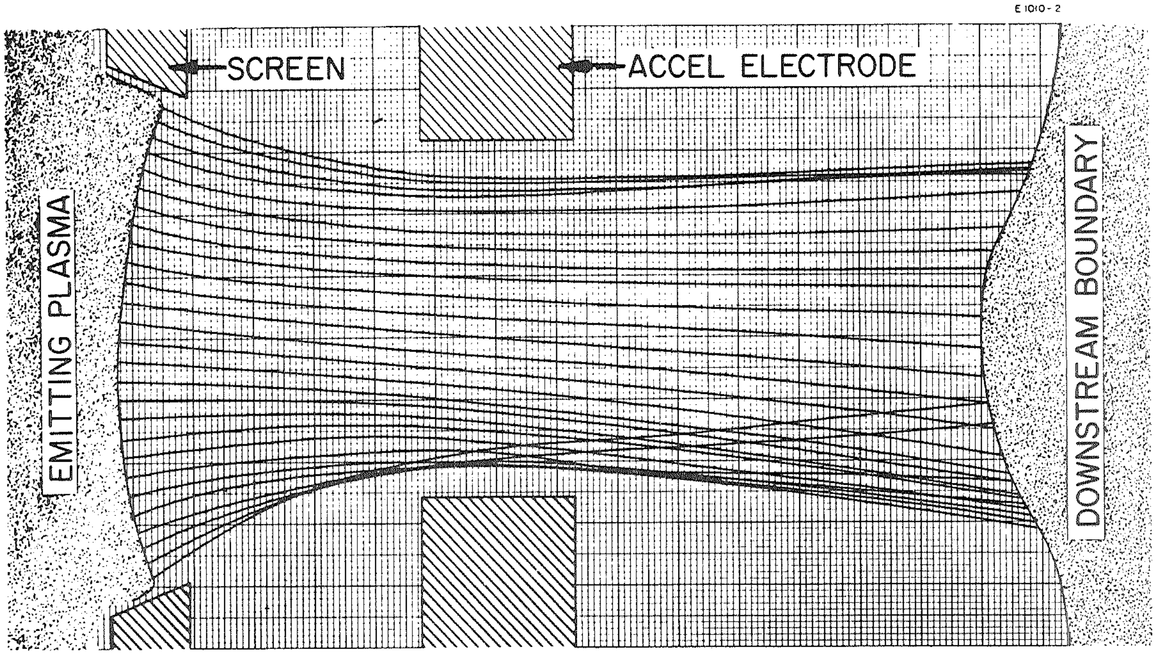

0.18 mm Displacement (5% of Accel Aperture), θ_{avg} = 4.1°.

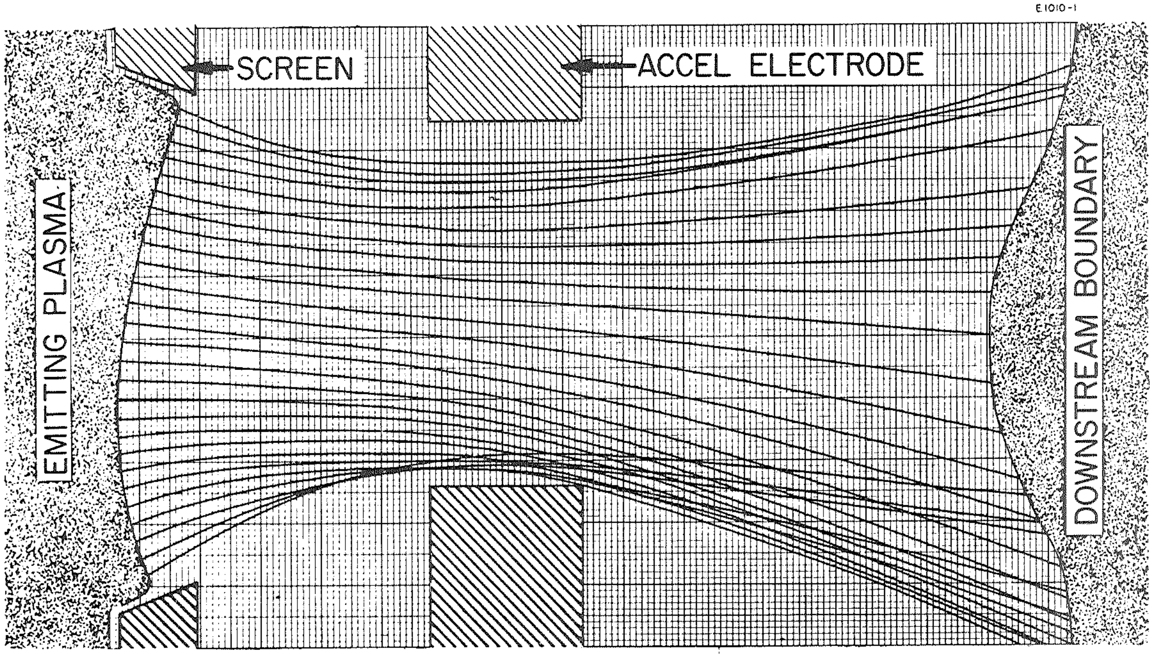

0.36 mm Displacement (10% of Accel Aperture), θ_{avg} = 8.2.

Fig. 9. Digital Computer Trajectory Calculations for Hg^+ Perveance = 5.6×10^{-9} A/V 3/2.

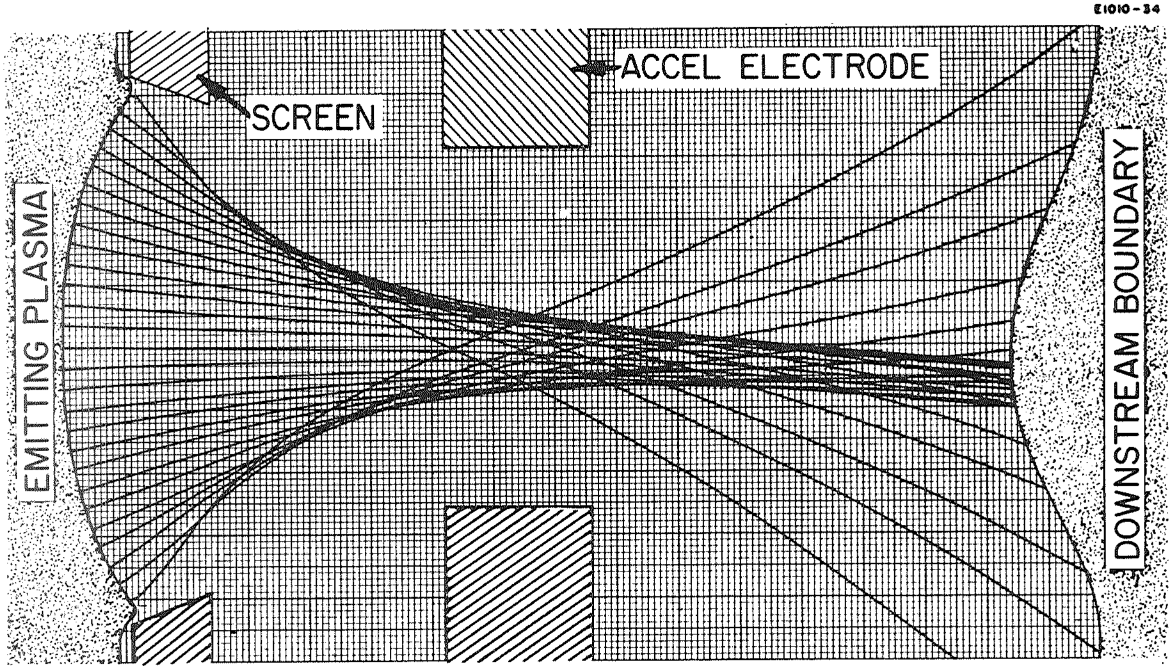

0.18 mm Accel Displacement (5% of Accel Aperture), θ_{avg} = 4.5

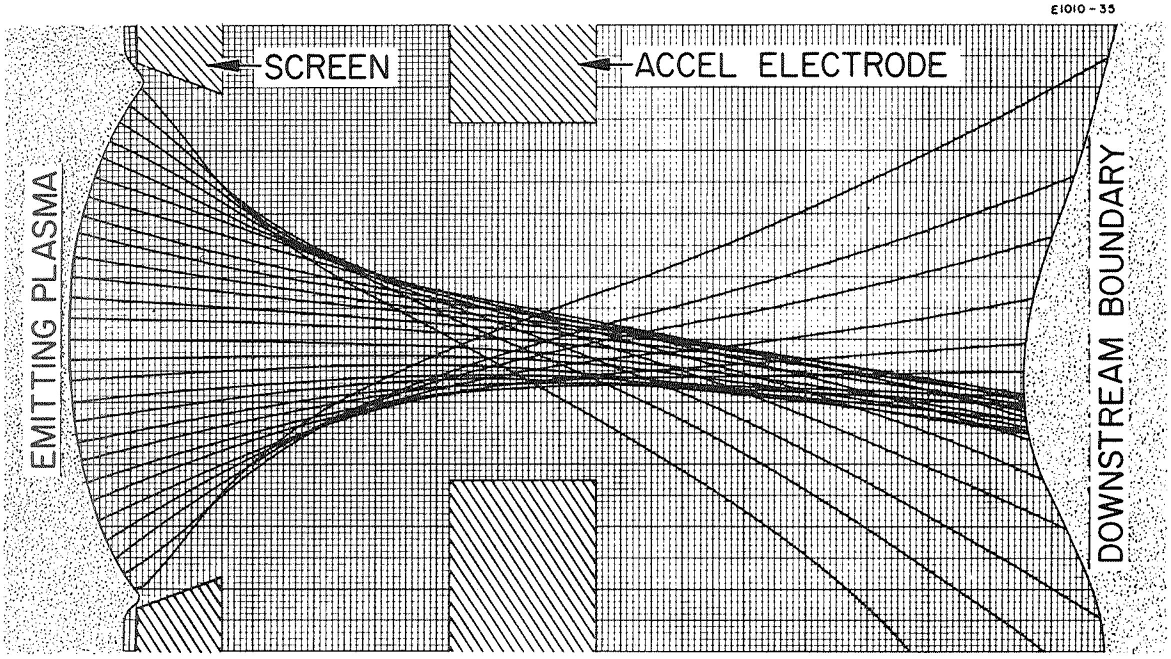

0.36 mm Accel Displacement (10% of Accel Aperture), θ_{avg} = 8.8

Fig. 10. Digital Computer Trajectory Calculations for Hg^+ Perveance = 1.6×10^{-9} A/V 3/2.

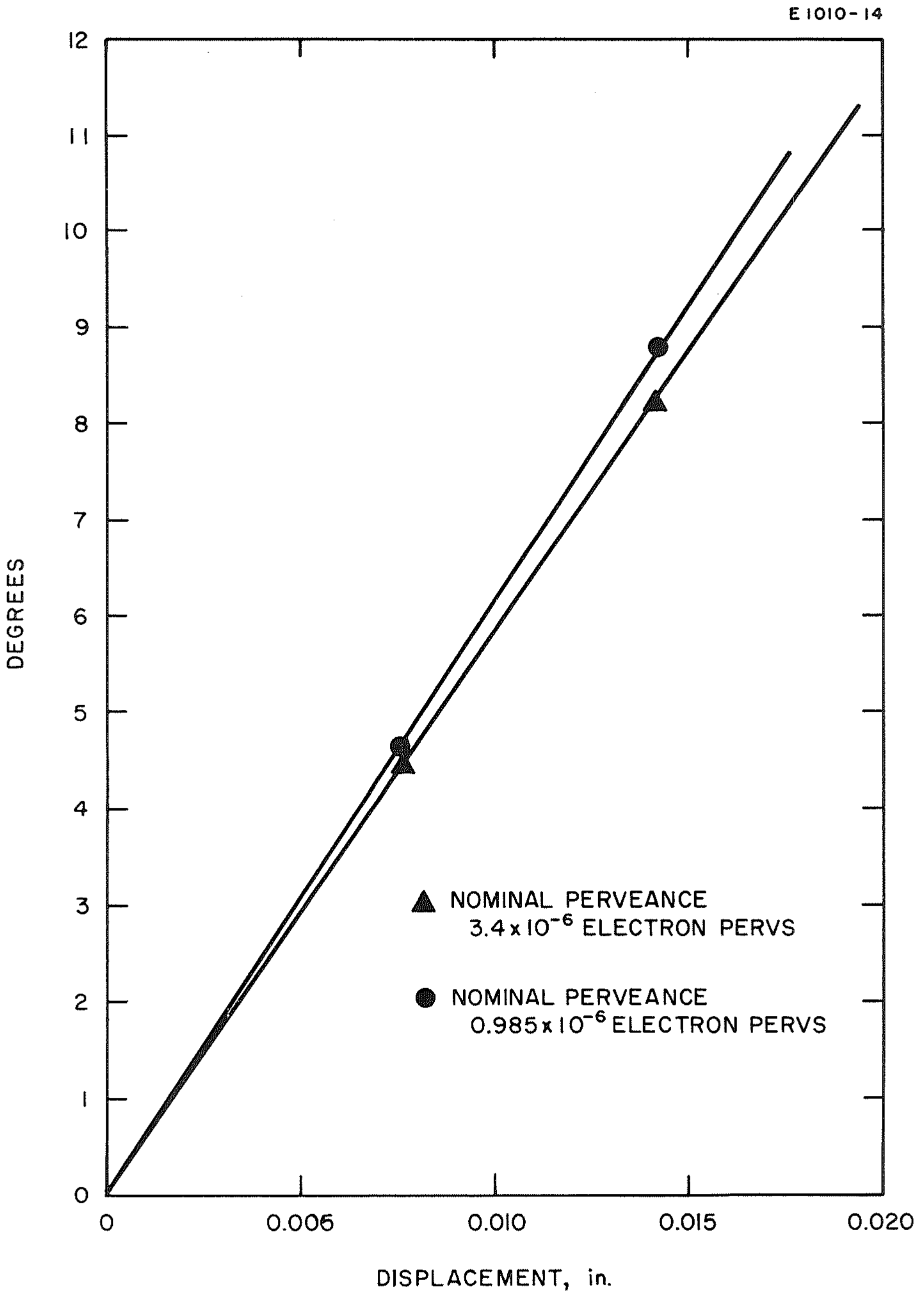

Fig. 11. Mean Angular Displacement of Ion Trajectories due to Transverse Displacement.

This latter figure agrees closely with the work of Lathem,[7] who found an angular displacement of 9.2 degrees for an accel displacement of 10% for a different electrode geometry. In the latter study, it was concluded that direct interception could be expected at an ion beam deflection angle of 16 degrees.

For a strip geometry, all the above average ion trajectory angles can be taken as the average thrust deflection angle, since to first order each trajectory line represents the same amount of ion current. However, when these results are to be applied to hole geometries, an integration must be performed which weights the outer beam trajectories more because they carry more current. In addition, for the hole geometry the amount of transverse displacement varies from a maximum value to a value of zero, 90 degrees away in azimuth. The detailed calculations taking into account these two factors have been performed in Ref. 6. The results are summarized in Table II.

TABLE II

CALCULATED AVERAGE DEFLECTION ANGLE AND MEAN THRUST DEFLECTION ANGLE FOR PLANAR AND AXIALLY SYMMETRIC GEOMETRIES

Nominal Hg^+ Perveance	Transverse Perturbation of Accel, mm	Planar Symmetry		Axial Symmetry
		Average Deflection Angle, deg	Mean Thrust Deflection, deg	Mean Thrust Deflection, deg
$5.6 \times 10^{-9} \frac{A}{V^{3/2}}$	0.18	4.1	4.1	2.9
	0.36	8.2	8.2	5.8
1.6×10^{-9}	0.18	4.5	4.5	2.5
	0.36	8.8	8.8	5.0

T145

When the maximum deflection angles found for these planar geometries are extrapolated to hole geometries, the ∿8 and 18 degree maximum deflection angles become equivalent to maximum mean thrust deflection angles of ∿5.8 and ∿10 degrees for the analogous axial symmetry.

While these computations indicated that this type of system should barely meet the design specifications of 10 degrees deflection, it was decided to construct such a device to experimentally verify the computed predictions. As shown in Section V-C the test results demonstrated that the predictions were very conservative and that thrust deflections of greater than 15 degrees were possible.

The mechanical design of the moving electrode system centered about two areas — the selection of an actuator to provide the force necessary to move the electrode and the design of a suspension system which preserved the interelectrode spacing but permitted transverse motion of the grid. The three most promising actuators considered were bimetal helical springs, thermally expanding coil springs, and an electromagnetic pump which could be used to expand a fluid filled bellows. After prototype tests of all three systems, it was found that the thermally actuated coil spring system was the most promising.

The basic design concept is shown in Fig. 12. The screen electrode is supported on four thin flexible columns which are strong in tension. The screen pole piece supports the electrode so that the columns cannot be compressed. This provides the necessary axial support without constraining the transverse flexibility.

The electrode is held in static equilibrium by pairs of stretched coil springs whose axes are transverse to the supporting columns.

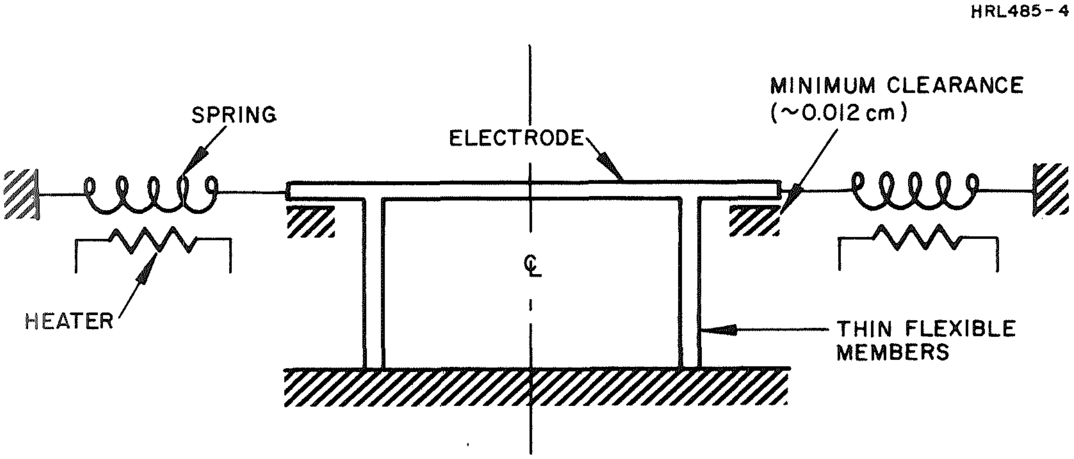

Fig. 12. Design Basis for Thermally Controlled Spring Actuator.

According to basic spring equations,[8] at equilibrium the relation between deflection and load force is given by

$$P = \frac{f\ Gd^4}{8\ D^3 N} \tag{2}$$

where

P = load (lb)
f = deflection (in.)
d = wire diameter (in.)
D = mean diameter of coil (in.)
N = number of active coils
G = shear modulus (psi).

Rearranging eq. (2), the spring constant K can be found

$$K = \frac{P}{f} = \frac{d^4 G}{8ND^3} . \tag{3}$$

Under a constant load P, it may be shown that the deflection will change with temperature according to eq. (4).

$$\Delta f = \frac{8\ ND^3 P}{d^4 G} \left(\frac{3\alpha\Delta T}{2} \right) . \tag{4}$$

In the actual system this idealized case is complicated by the fact that the load P is supplied by a spring and hence decreases as the length of the spring changes. In addition, the load on the heated spring is further reduced by the force required to bend the support wires. The net deflection is thus less than predicted by eq. (4), but is still adequate to provide the necessary electrode motion. It may be shown that the amount of deflection can be computed by eq. (5).

$$\Delta \ell = \frac{3\alpha\ \Delta T\ f_o}{2 + \frac{nK_2}{K_1}} \tag{5}$$

where

$\Delta \ell$ = net electrode deflection (in.)
α = coefficient of linear expansion (per °C)
ΔT = temperature change (°C)
f_o = initial spring deflection (in.)
n = number of support wires
K_1 = spring constant of helical spring (lb/in.)
K_2 = spring constant of support wire (lb/in.)

In actual operation the spring is heated directly by passing current through it. Test results of a spring element made of ELGILOY cobalt-nickel alloy are shown in Fig. 13. ELGILOY maintains its mechanical characteristics, such as tensile strength, modulus of elasticity, and torsional modulus up to 600°C. A typical data point taken from Fig. 13 resulted in a deflection of 2.2 mm for a temperature change of 200°C under a 1.0 kG load at a power expenditure of 3.5 W in air. No support wires were present during this test. The spring can be designed to fit a particular application to provide a specific deflection for a given load and ΔT by varying the wire diameter, coil size, preload, and number of turns according to eq. (4). The electrical resistance of the spring can be adjusted by changing the wire diameter and length.

Figure 14 is a photograph of a movable screen electrode system whose design is based on the above concepts.

C. VECTORABLE DISCHARGE CHAMBER SYSTEM

This concept evolved from the premise that it would be much easier to gimbal the relatively light discharge chamber and ion extraction system, but difficult to support and

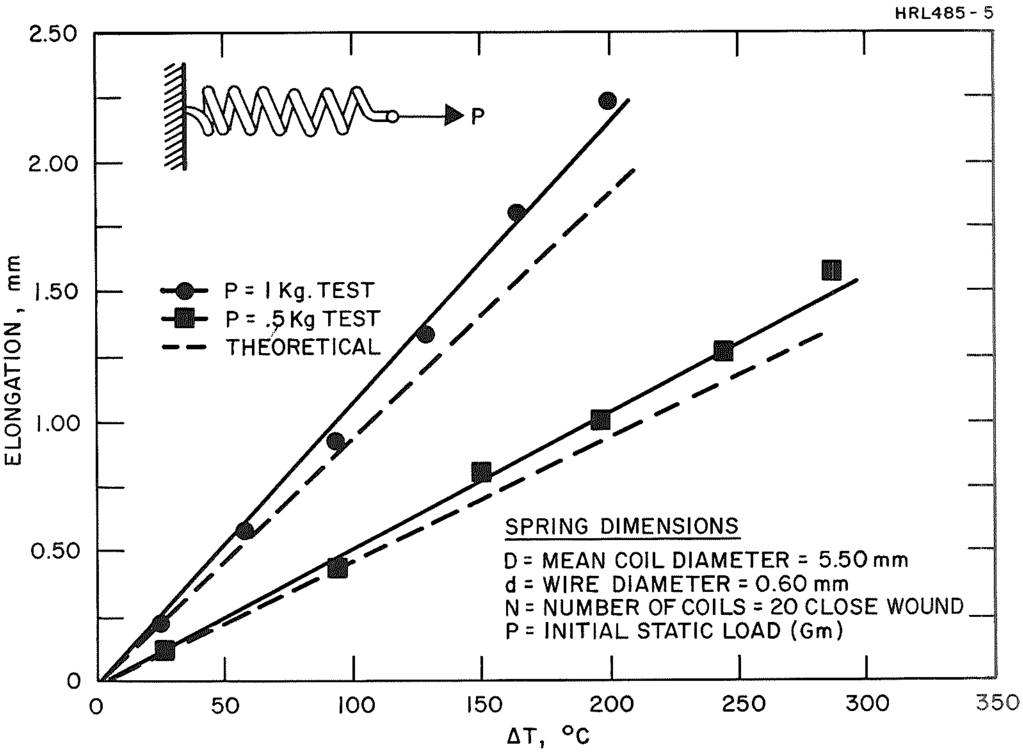

Fig. 13. Strength of ELGILOY Coil Springs as a Function of Temperature.

M 7548

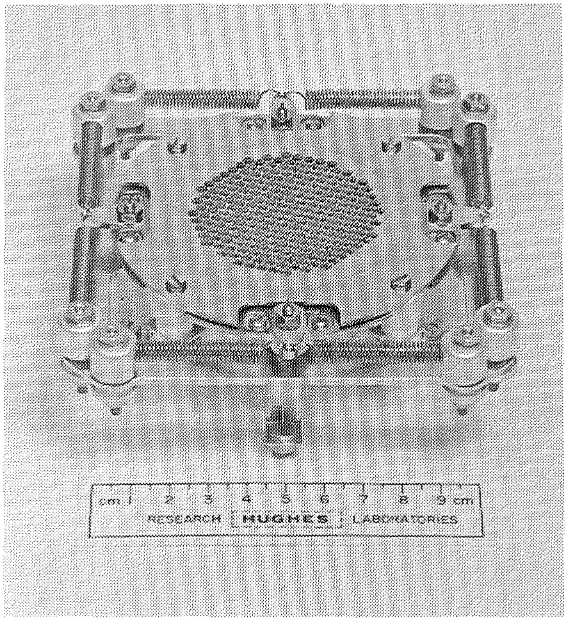

Fig. 14.
Movable Screen Electrode System (Downstream Side).

precisely control the heavy propellant storage tank. Since the propellant feed line which connects the two is a thin flexible member, the two parts of the system are essentially mechanically decoupled, thus simplifying the design. The advantage of such a system is that the thruster performance should be in no way perturbed from that of a nonvectorable system.

An initial attempt was made to construct a system of this design using the thermally actuated coil springs described above as actuators. Even with short moment arms a relatively long spring travel was required to provide the necessary 10 degree deflection. This could not be achieved due to the reduction in driving force of the opposing unheated spring as it reduced in length (see Section III-B). The design was successfully modified to employ a spherical bearing and a vacuum qualified stepper motor and cam to provide the necessary motion. This provided a discrete repeatable array of deflection angles.

A functional mockup is shown in Fig. 15.

M 7501

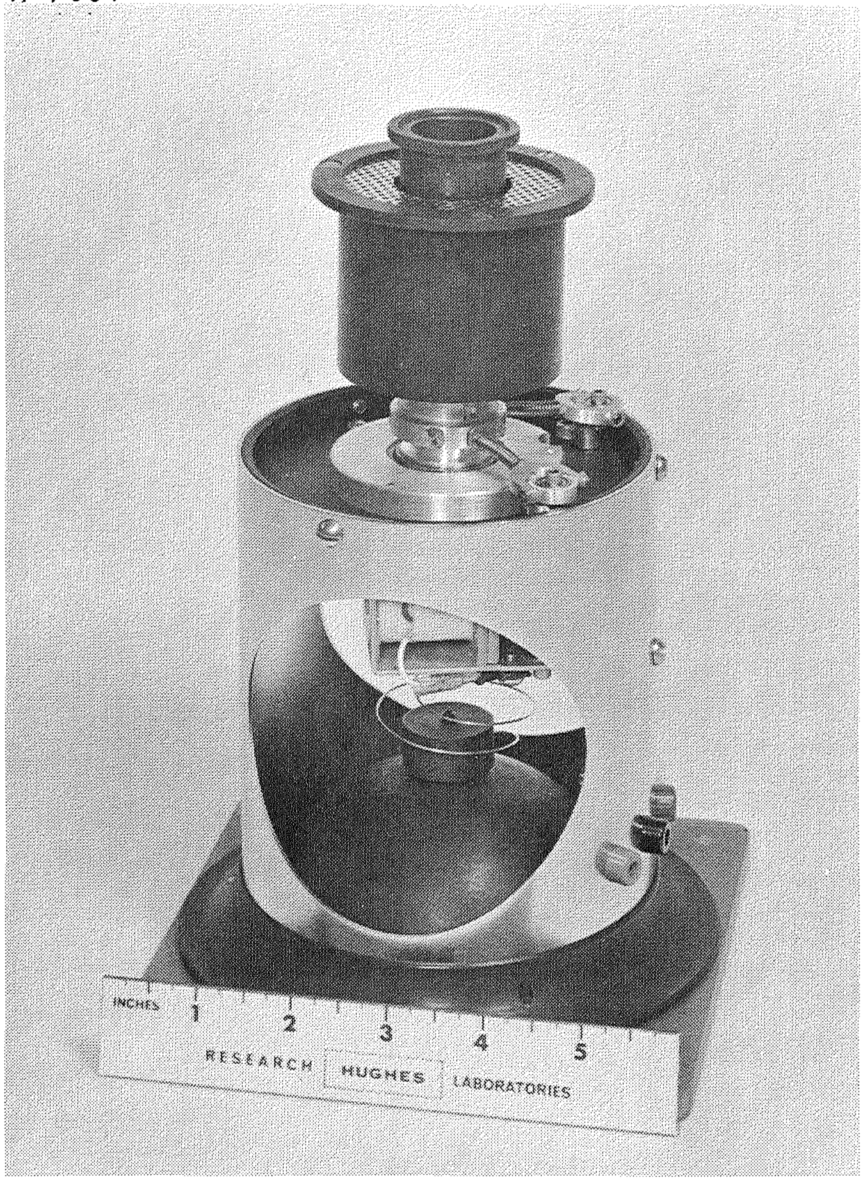

Fig. 15. Vectorable Discharge Chamber System Mockup.

SECTION IV

TEST AND DATA PROCESSING FACILITIES

Performance evaluation of the various ion optical systems required detailed documentation of the beam current density over an array of selected points in a series of planes perpendicular to the nominal beam axis. This required the design and construction of a movable Faraday cup prove whose position could be controlled remotely from outside of the chamber. It was also found necessary to adapt a computerized data analysis technique to process the large quantities of numerical results generated by an automated system of this type.

A. VACUUM SYSTEM AND POWER CONDITIONING

All tests were conducted in a 1.5 m diameter by 4.6 m long vacuum chamber equipped with a cylindrical cryoliner and a water cooled beam collector as illustrated in Fig. 16. The thruster is mounted from the end bell so that it is completely exposed to the cryoliner and the beam is not apertured by any port or valve. A conventional electronic test setup was used with the common point of the positive and negative high voltage supplies and the neutralizer coupled to ground through zener diodes to assure a neutralizer emission equal to the beam current without permitting this common point to float to high voltage in the event of neutralizer failure.

The deflection supply used for the electrostatic deflection tests was especially constructed for this program. It consisted of four voltage sources ganged in pairs to provide differential voltages in each of the x- and y-directions. The circuit and metering are illustrated in Fig. 17.

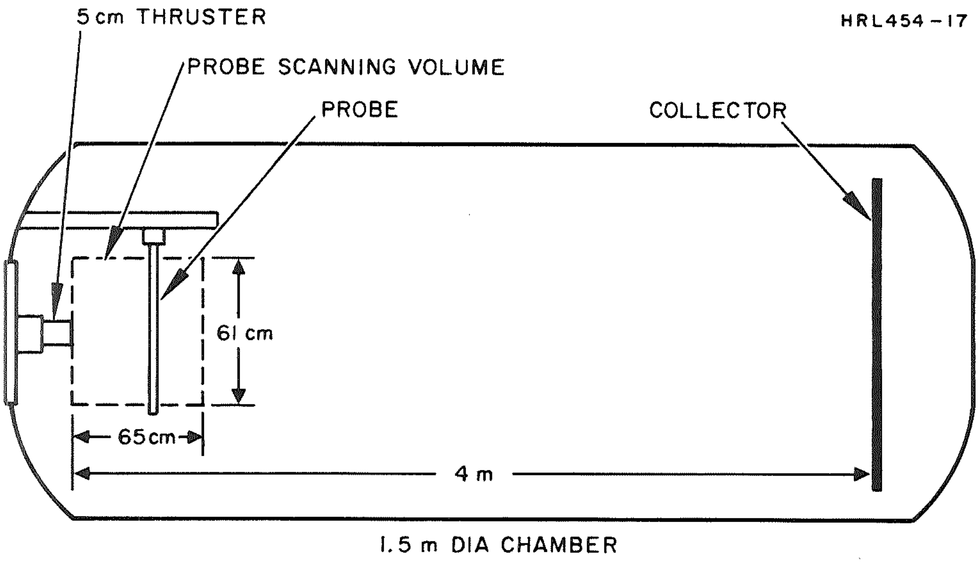

Fig. 16. Schematic of 1.5 m Test Facility.

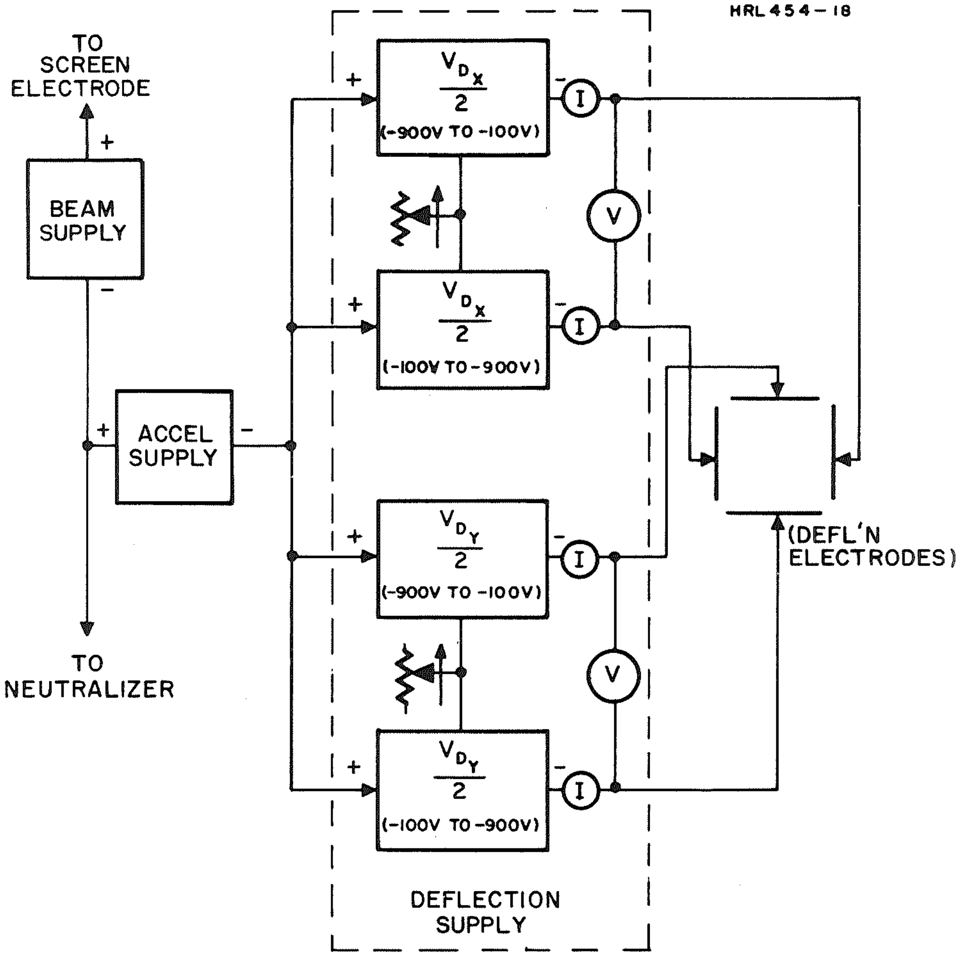

Fig. 17. Functional Diagram of Deflection Power Conditioning Used with Electrostatic Systems.

B. BEAM PROBE AND DATA ANALYSIS

A rather sophisticated beam probe shown in Fig. 18 was constructed for this program. The 65 cm long probe which appears as a vertical rod in Fig. 18 contains 35 individual Faraday cups behind 0.16 cm diameter apertures. (In the tests only 13 cups were used to reduce the data collection time.) The probe carrier runs on two tracks that allow it to be positioned in the Z (parallel to the chamber centerline) and X (horizontal and perpendicular to chamber centerline) directions by two pulse driven stepper motors actuated from outside the tank. Thus, the beam intensity may be sampled within the volume downstream of the thruster over the range of $X = \pm 33.4$ cm, $Y = \pm 30.5$ cm, and $z = 3.2$ to 64.8 cm from the accelerator electrode.

Circuitry was provided to automatically step the probe carrier in the X and Z directions. A data acquisition system, shown schematically in Fig. 19, was used to measure the magnitude of the beam current samples collected in the probe cups and automatically record this information on punched tape which could be then fed directly into the computer for analysis. In operation a typical scan consisted of setting the probe carriage at the desired Z distance and then scanning each of 13 Faraday cups at 13 preselected equally spaced positions in the X direction. Such a scan took approximately 6-1/2 min to perform.

The analysis of the data consisted of using the computer to fit a three-dimensional surface to the beam intensity measurements taken in a particular plane. The computer calculates the x and y position of the centroid of the volume defined by this surface, the magnitude of the total current represented by the surface and the location of the curves of

M 7274

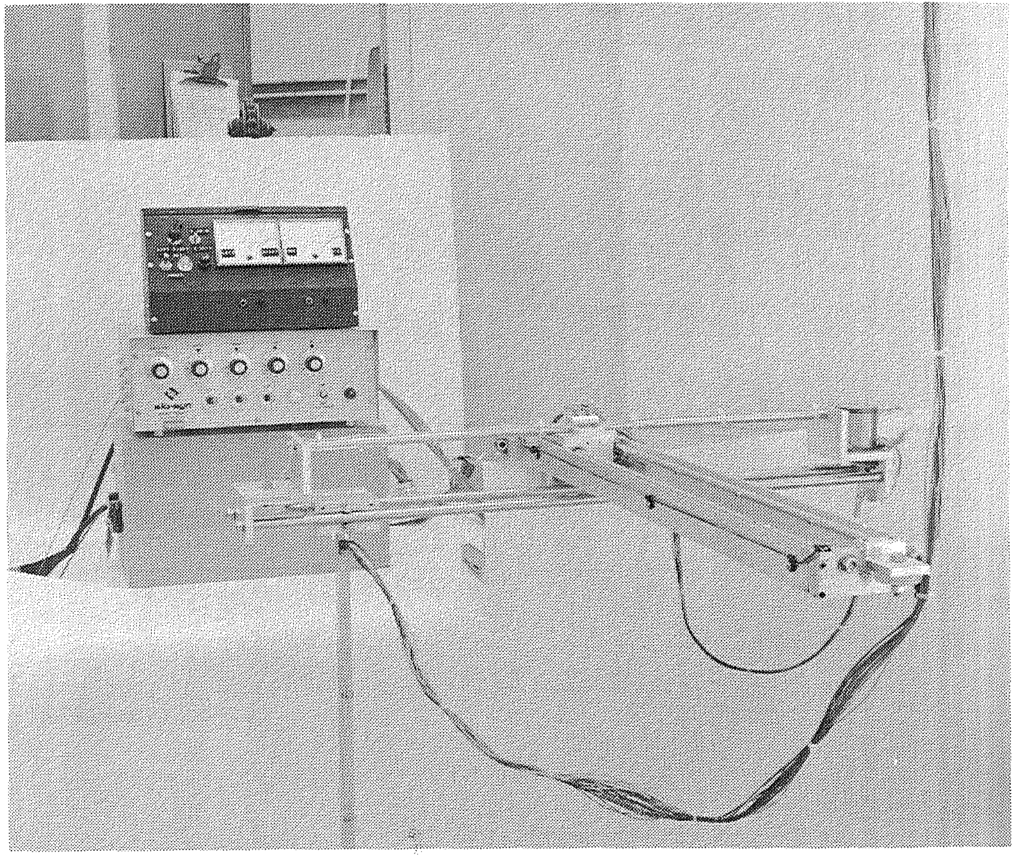

Fig. 18. Beam Vector Probe and Data Acquisition Equipment.

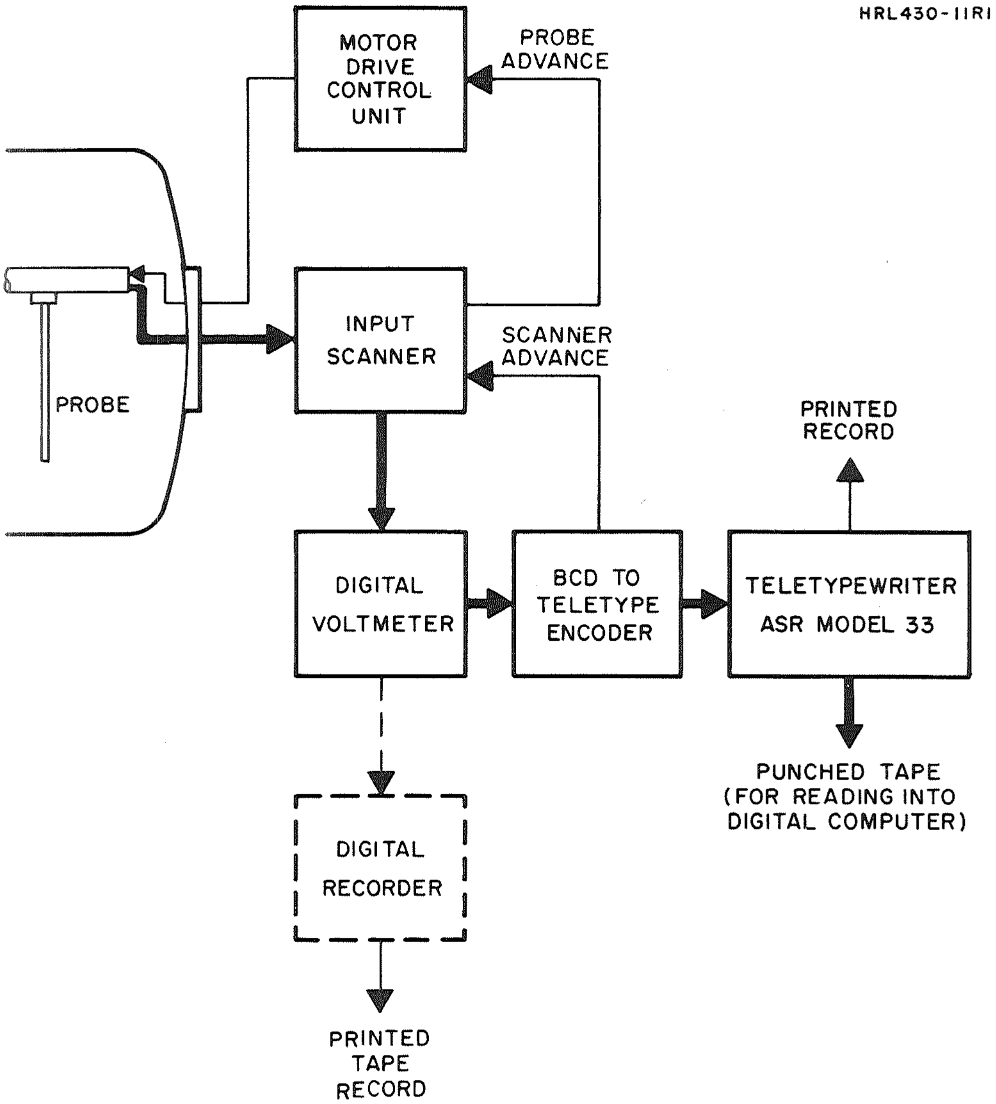

Fig. 19. Functional Diagram of Data Processing System.

equal current intensity over the surface. These latter contours can be automatically plotted by the computer using a Calcomp plotter, as shown in Fig. 20. This was done periodically to check the beam shape, but too much time was needed (approximately 20 min/plot) to do each of the more than 400 scans taken during this program.

Although somewhat laborious to construct and debug, this automated data collection and processing system proved of considerable value in expediently completing the performance mapping of the various deflection systems.

MOVABLE SCREEN ELECTRODE SYSTEM

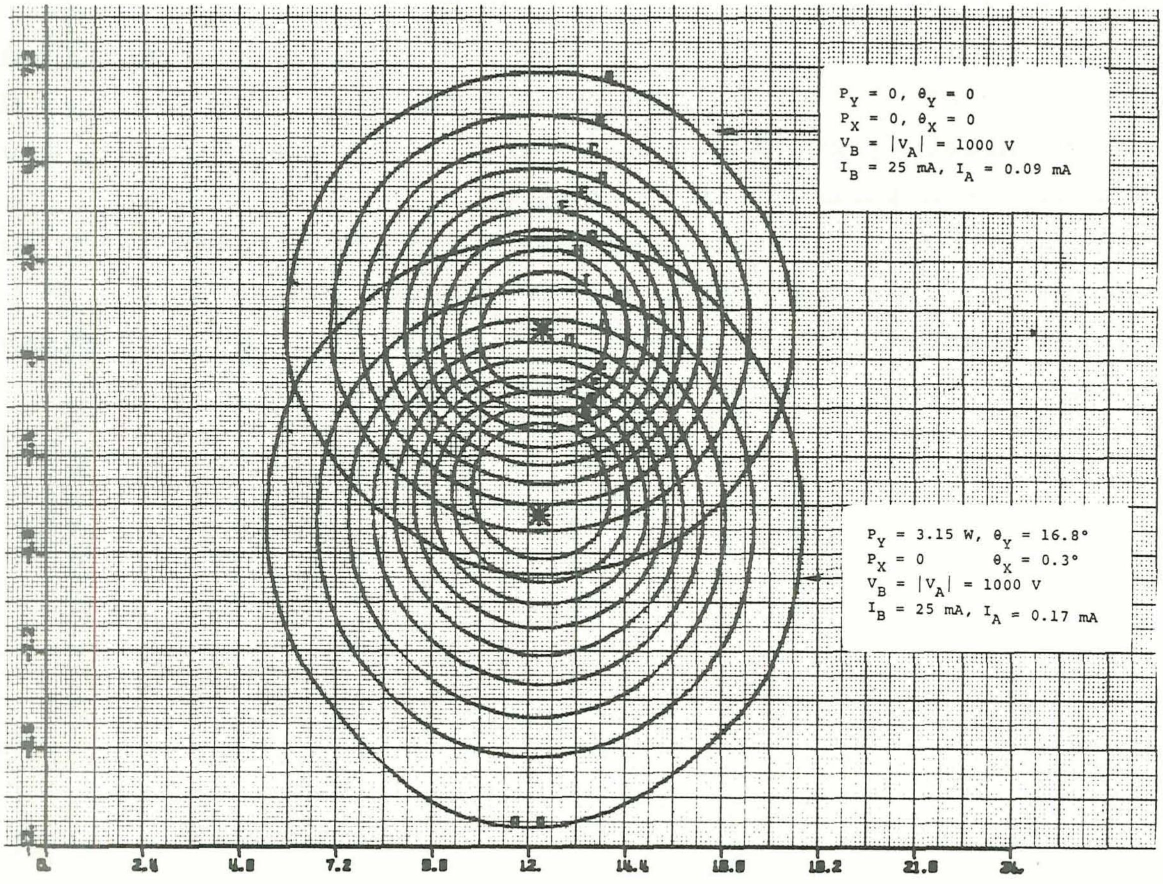

Fig. 20. Typical Beam Intensity Contours Showing Normal and Deflected Beams.

SECTION V

EXPERIMENTAL COMPARISON OF SYSTEM PERFORMANCE

The statement of work places the following boundary conditions on the operating point:

- Net accelerating voltage: 500 to 2000 V
- Total accelerating voltage: 600 to 3000 V
- Thrust: 0.25 to 1.0 mlb
- Propellant utilization efficiency: 60 to 80%.

These boundaries are displayed graphically in Fig. 21. Here we have assumed an accel-decel ratio of 2 although this is in reality also a variable.

An additional factor that affects the amount of current that may be extracted at a given total voltage is the beam current density profile which is governed by the plasma density in the discharge chamber. The uniformity of this plasma density across the discharge chamber diameter also affects the direct ion impingement on the accelerator as a function of deflection angle. This is due to the imperfectly focused crossover trajectories near the periphery of the beam where the current density is low and the poorly converged trajectories at the central apertures where the current density is highest. Clearly a perfectly flat plasma profile would permit an "optimum" total extraction voltage which would focus all beamlets equally well. It is not possible to compensate for the nonuniformity of the plasma by adjusting the aperture diameters because of construction difficulties in the "eggcrate" design. Neither is it practical in the moving screen electrode system because the deflection angle depends on the distance that the electrode is displaced expressed as a fraction of the screen aperture diameter and would thus be different for each aperture size.

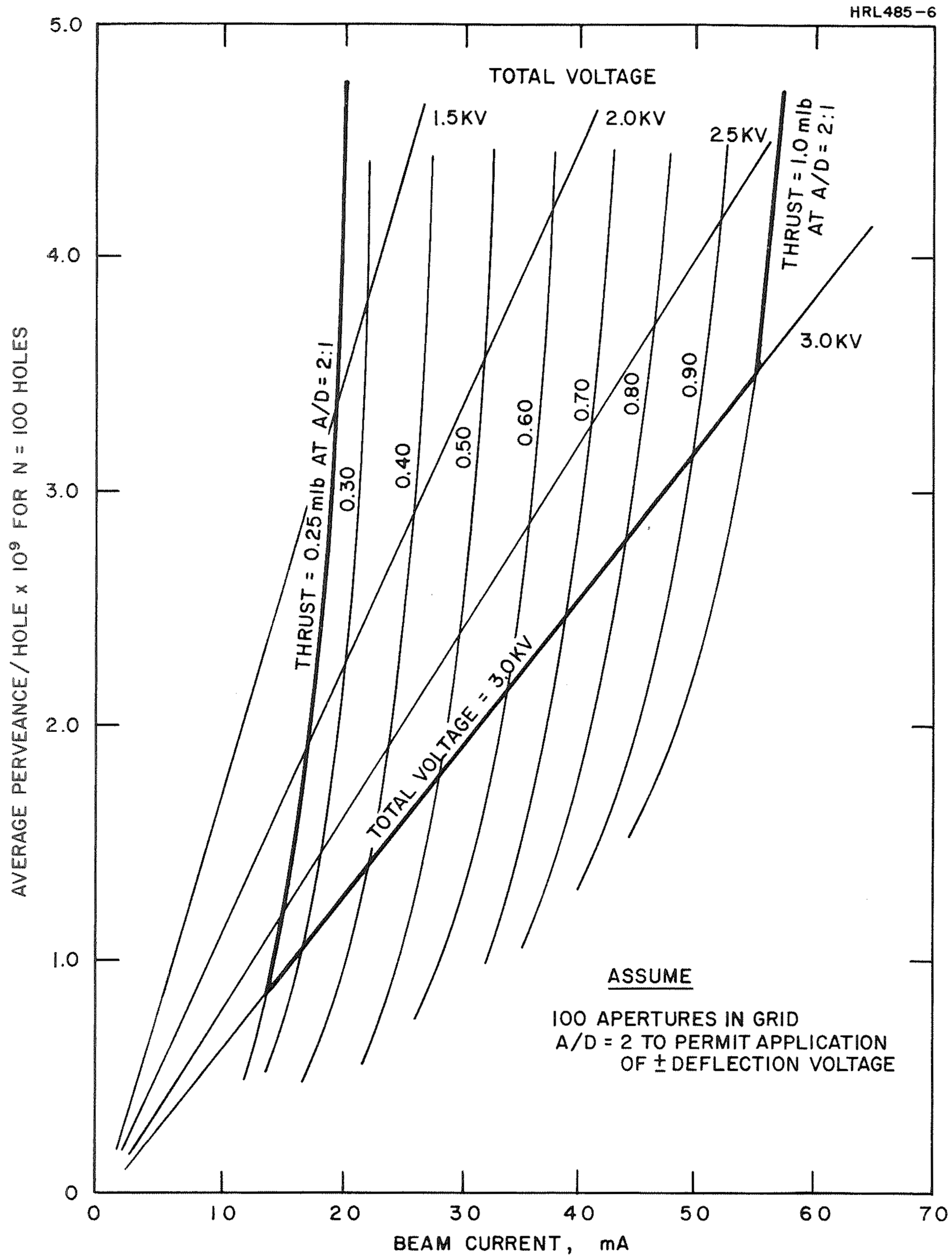

Fig. 21. Contractually Specified Design and Operating Limits for 5 cm Thruster.

The experimental procedure used was to establish a neutralized beam current in the range from 25 to 30 mA and to measure the accelerator current as a function of total extraction voltage ($V_+ + |V_-|$). This curve generally had the form of a broad minimum, such as shown in Fig. 22, because of the summation of the direct interception currents from underfocused trajectories near the center of the beam, which occur at the lower voltages, and the crossover trajectories near the edge of the beam, which occur at the higher voltages. A third drain current component is, of course, created by charge exchange ions. A total voltage near the upper permissible limit was usually chosen so as to minimize the diameter of the beamlets near the center of the thruster. The relatively high total voltage was also required when electrostatically deflecting because the deflecting voltage (V_d) was applied across the apertures so that one deflecting electrode had the potential $V_- + (V_d/2)$ and the other $V_- - (V_d/2)$. The smaller of these two must still provide sufficient voltage to stay to the right of the perveance line.

Once the operating point was established, a series of deflecting voltages were applied and beam probe scans taken to accurately establish the deflection angle. Profiles were measured at several axial distances to remove any ambiguity which might arise as a result of initial misalignment of the thruster.

A. ELECTROSTATIC DUAL GRID SYSTEMS

Four configurations of electrostatic dual grid deflection systems were tested. One system included alumina spacing strips brazed between the deflection electrodes. The other

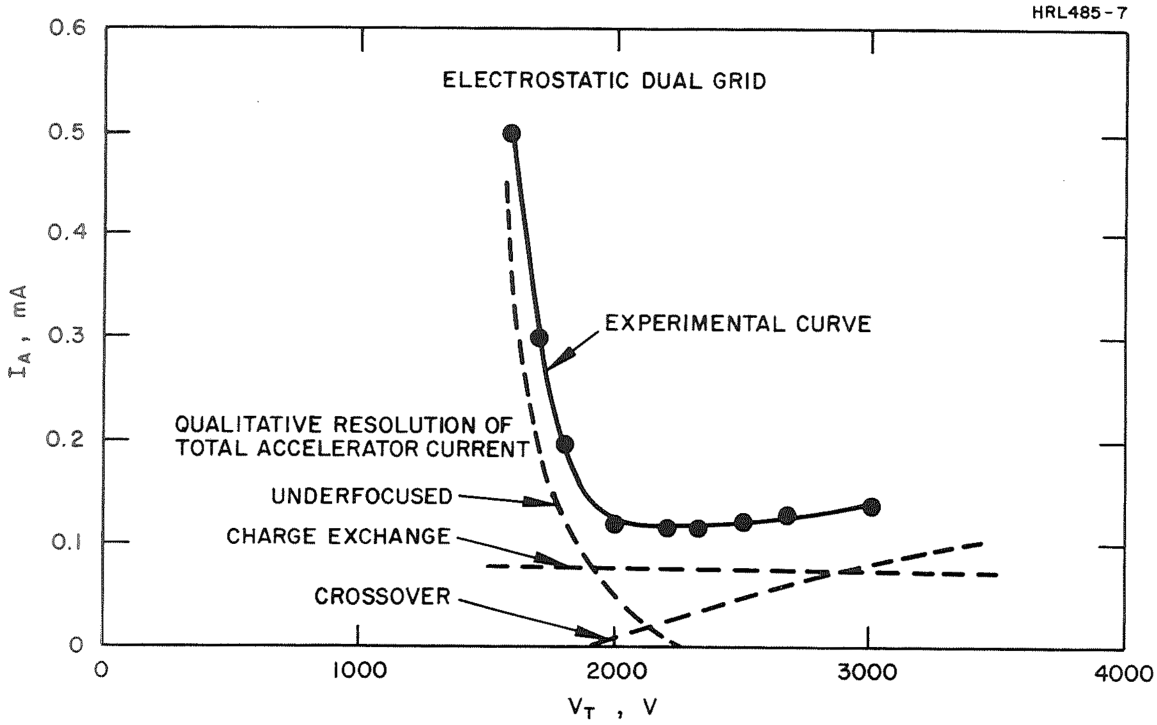

Fig. 22. Constituents of Accelerator Current as a Function of Total Voltage.

three systems were assembled with ceramic spacing disks at the ends of the electrodes outside the active beam region. The latter three systems differed in accel electrode dimensions and shape and grid spacing. The four systems are identified and described in Table III.

1. System A (with Interelectrode Insulators)

Although considerable effort was expended in the design of the electrodes to sputter shield the exposed surfaces of the ceramic strips, the useful lifetime of this system was only two hours due to the accumulation of sputtered material on the interelectrode insulators. The system was tested, disassembled, cleaned, and retested with similar results. The deflection results obtained during this time are presented in Table III.

A number of solutions to the problem of interelectrode insulator shorting were proposed and tried. The best solution was to remove the insulating strips from the eggcrate structure entirely and support the metal electrodes only from the ends. Thus, Systems B, C, and D were built without the ceramic interelectrode insulating slabs.

2. Systems B, C, and D (No Interelectrode Insulators)

As shown in Table III, the differences between systems B, C, and D are in the dimensions and shape of the accel electrode and the spacing between screen and accel grid. System B was assembled from parts which were on hand when the decision was made to eliminate the interelectrode insulating strips. Testing of this system without any interelectrode shorting demonstrated that the eggcrate structure with the electrodes supported only at the ends was structurally sound. Both the direct interception and deflection sensitivity of this system were high (see Table III), because of the high L/D ratio.

TABLE III

DUAL GRID ELECTROSTATIC SYSTEMS COMPARISON

System	Screen Aper., cm	Accel		Accel L/D	Grid Spacing, cm	V_I, V	V_A, V	V_T, V	I_B, mA	I_A, mA	eV/ion	η_{md}, %	X-Axis Deflection Sensitivity (deg/volt)
		Length L, cm	Aper. D, cm										
A (S/N 101 with insulating strips)	0.391	0.305	0.343	0.89	0.178	1600	1000	2600	15	0.11	—	—	0.011 (one data point)
B (prototype)	0.391	0.445	0.318	1.4	0.109	1420	1200	2620	25	0.78	420	66.0	0.025
C (S/N 101 without insulating strips)	0.391	0.305	0.343	0.89	0.178	1300	1300	2600	25	0.25	446	63.8	0.012
D (S/N 104)	0.391	0.254	0.343	0.74	0.127	1000 1200	1000 1200	2000 2400	25 30	0.19 0.21	504 528	60.5 64.5	0.018 0.014 0.013[a]

[a] Adjusted to V_T = 2600 V.

T146

After 24 hours of testing there was significant erosion of the accel electrodes. Some of the strips had notches cut into them extending up to approximately 25% of the electrode width of 0.445 cm.

The second system without insulating strips (System C) was made with the same size and shape electrodes as System A. The shorter deflection length of these electrodes reduced the erosion and accel current. However, these electrodes still had the L shape initially introduced to provide sputter shielding of the insulating strips between the electrodes. Most of the erosion occurred on the edge of the downstream sputter shield which was perpendicular to the beam (see Fig. 23). The deflection sensitivity was similar to the limited results obtained with System A.

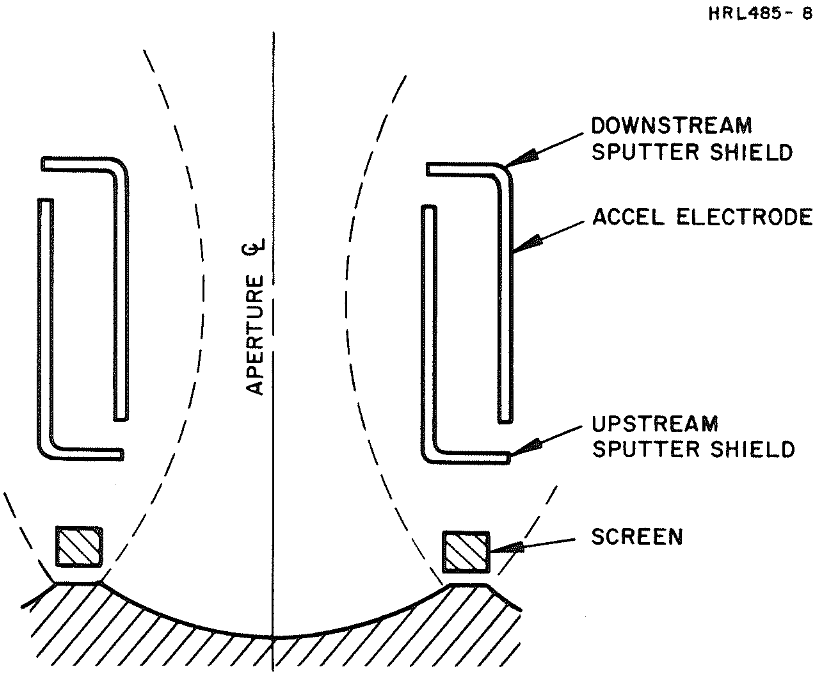

Fig. 23. Cross-Section of Dual Grid Electrostatic Aperture.

The final electrostatic dual grid system tested (System D) was made with straight electrodes that had a stiffening rib formed along the length of the electrode (see Fig. 5). Tests with this system resulted in slightly higher deflection sensitivity and slightly lower accel current than experienced with the System C.

The test parameters of interest for the dual grid electrostatic deflection systems were:

- Deflection sensitivity as a function of electrode dimensions
- Deflection sensitivity as a function of total accelerating voltage and beam current
- Maximum deflection angle as defined by either direction interception or interelectrode current.

The deflection sensitivity of the four systems tested is presented in Table III and Fig. 24. Using the slopes of the lines in Fig. 24, the values for k_{eff} in eq. (1) (ref. Section III-A) are found to be 0.80, 0.64, and 0.80 for Systems B, C, and D, respectively, thus indicating that this equation accurately accounts for variations in L/D over at least the factor of two represented by Systems B and D. The somewhat anomalous results for System C (larger L/D than system D, but lower sensitivity) is attributed to the L shape of the electrodes. With this shape electrode, the sections perpendicular to the beam (see Fig. 23) introduce a counteracting potential into the adjacent deflection region. The effective L distance is thus less than the physical length of the electrode. For comparison purposes Fig. 24 shows the + X axis deflection results for the four systems tested. The single data point for System A was obtained under high interelectrode current conditions using batteries instead of the deflection power supply.

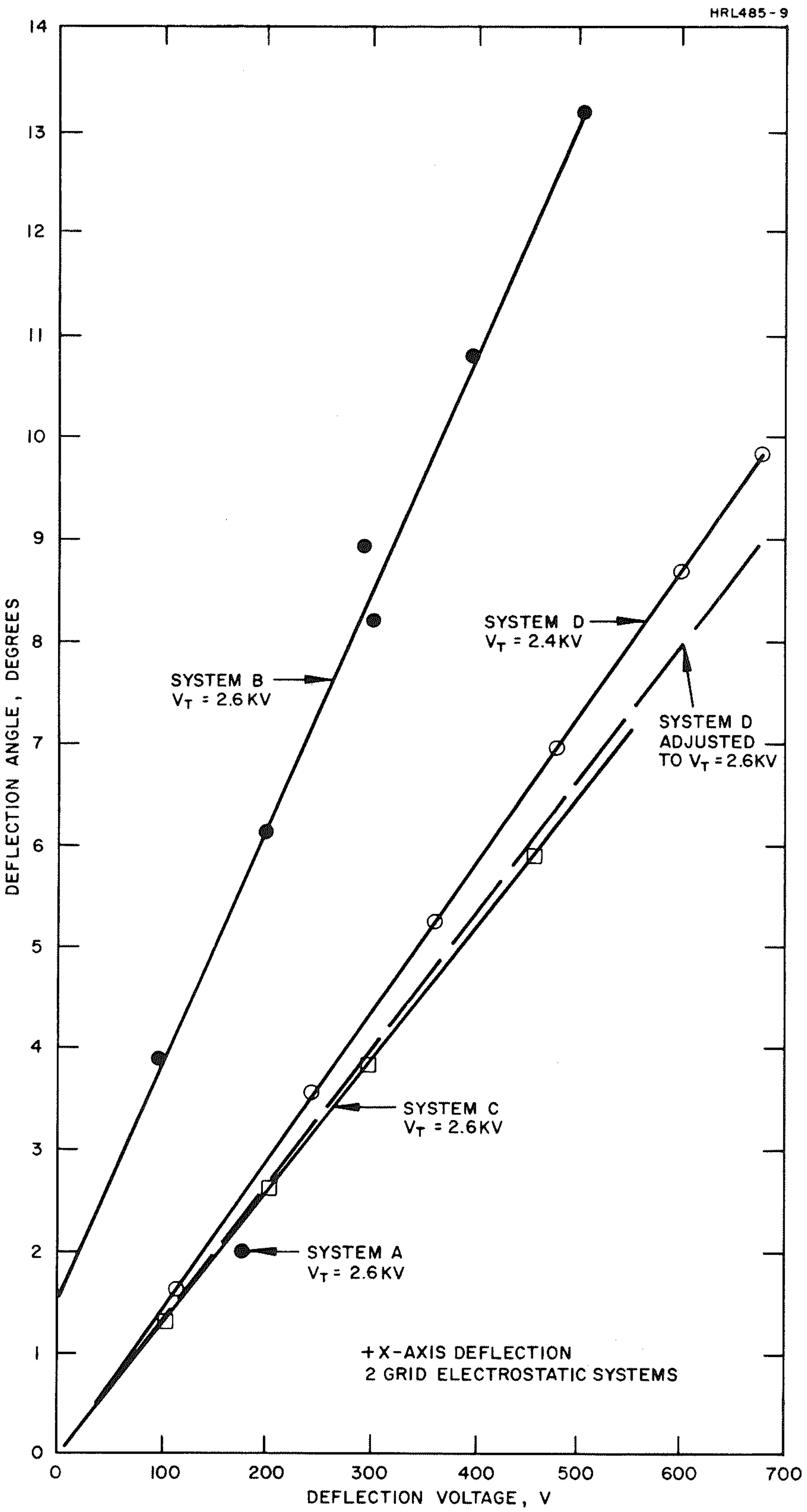

Fig. 24. Deflection Angle Versus Deflection Voltage for Dual Grid Systems.

The effect of total voltage and variations in beam current were examined by mapping System C over the range of V_T (2.0, 2.5, and 3.0 kV) and beam current (20, 25, and 30 mA) shown in Fig. 25. The effect on deflection sensitivity due to changing the total voltage is shown in Fig. 26. The deflection sensitivity of System D at two different total voltages is also shown in Fig. 26. Good agreement with the values predicted by eq. (1) are found using the values of k_{eff} calculated from Fig. 24.

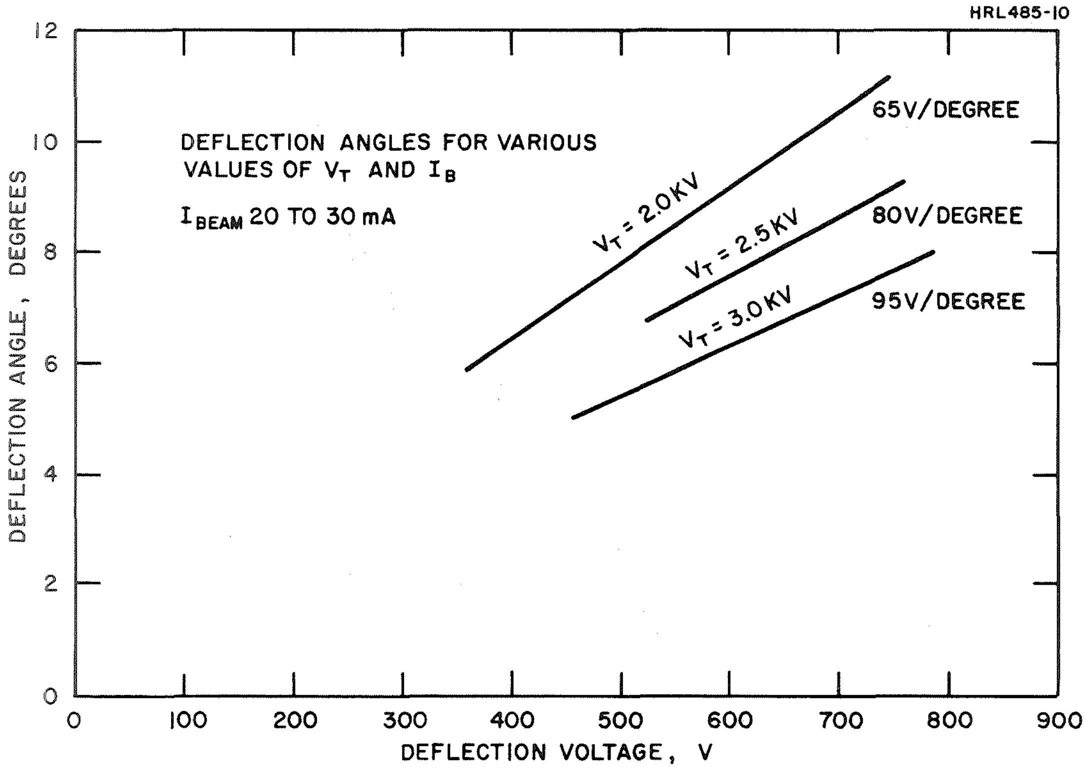

Fig. 25. Deflection Angle versus Deflection Voltage for 20 to 30 mA Beams.

The results of varying the beam current are shown in Fig. 25. At a total voltage of 2.5 kV the deflection results were the same for all three beam current levels. At a total voltage of 3.0 kV a ±3% spread in deflection angle was measured for the three beam currents at two different deflection voltages.

One variation in deflection sensitivity was observed that had not been predicted. It was discovered that the sensitivity was not the same for both axes. For instance, the average sensitivities for three days of testing of System D (at 2.4 kV) were 0.015 deg/V in the X axis and 0.011 deg/V in the Y axis. The deflection results shown in Fig. 27 illustrate this difference. A possible explanation of this is the physical asymmetry of the location of the notches in the electrodes required to permit assembly of the eggcrate structure. All of the individual strips lying in the same direction must have the notches facing the same way (see Fig. 5). Therefore, all of the electrodes that cause deflection along a given axis must either have the notches in the upstream or downstream edge of the electrodes. The edge of the electrodes with the notches would be expected to reduce the deflection when in the upstream position. System D was mounted on the thruster with the notches on the upstream side of the Y axis deflection electrodes.

The relation between accelerator current and deflection angle is presented in Fig. 28 which shows data for System D at two different operating points, plus some data obtained on a similar system at LeRC. The interesting features of the data presented in Fig. 28 are that at the lower level of total voltage and beam current, the I_A versus deflection angle curve exhibits the expected behavior; increasing accel current with increasing deflection angle. However, at the higher total voltage and higher beam current operating point, the accel

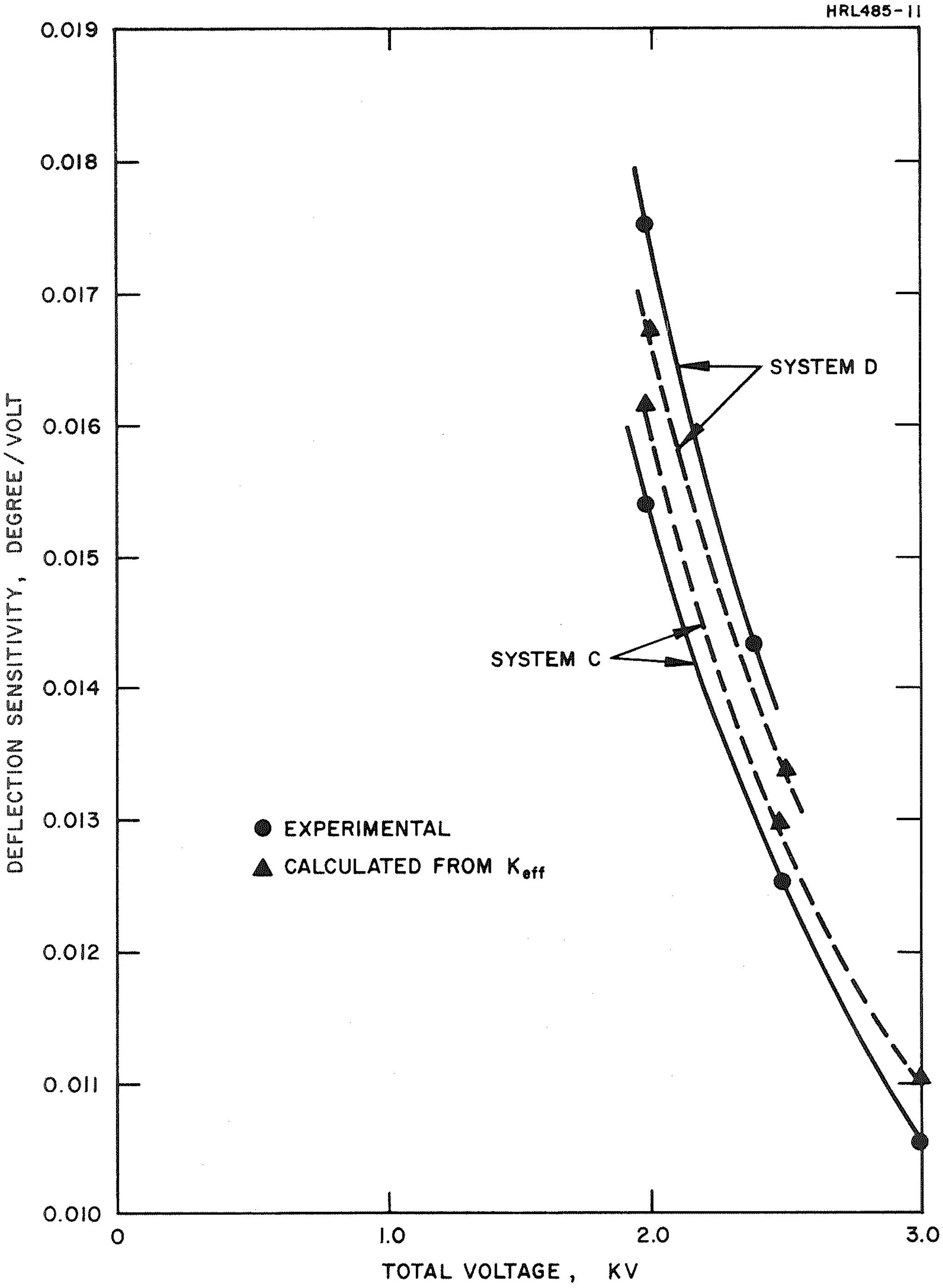

Fig. 26. Deflection Sensitivity Versus Total Voltage.

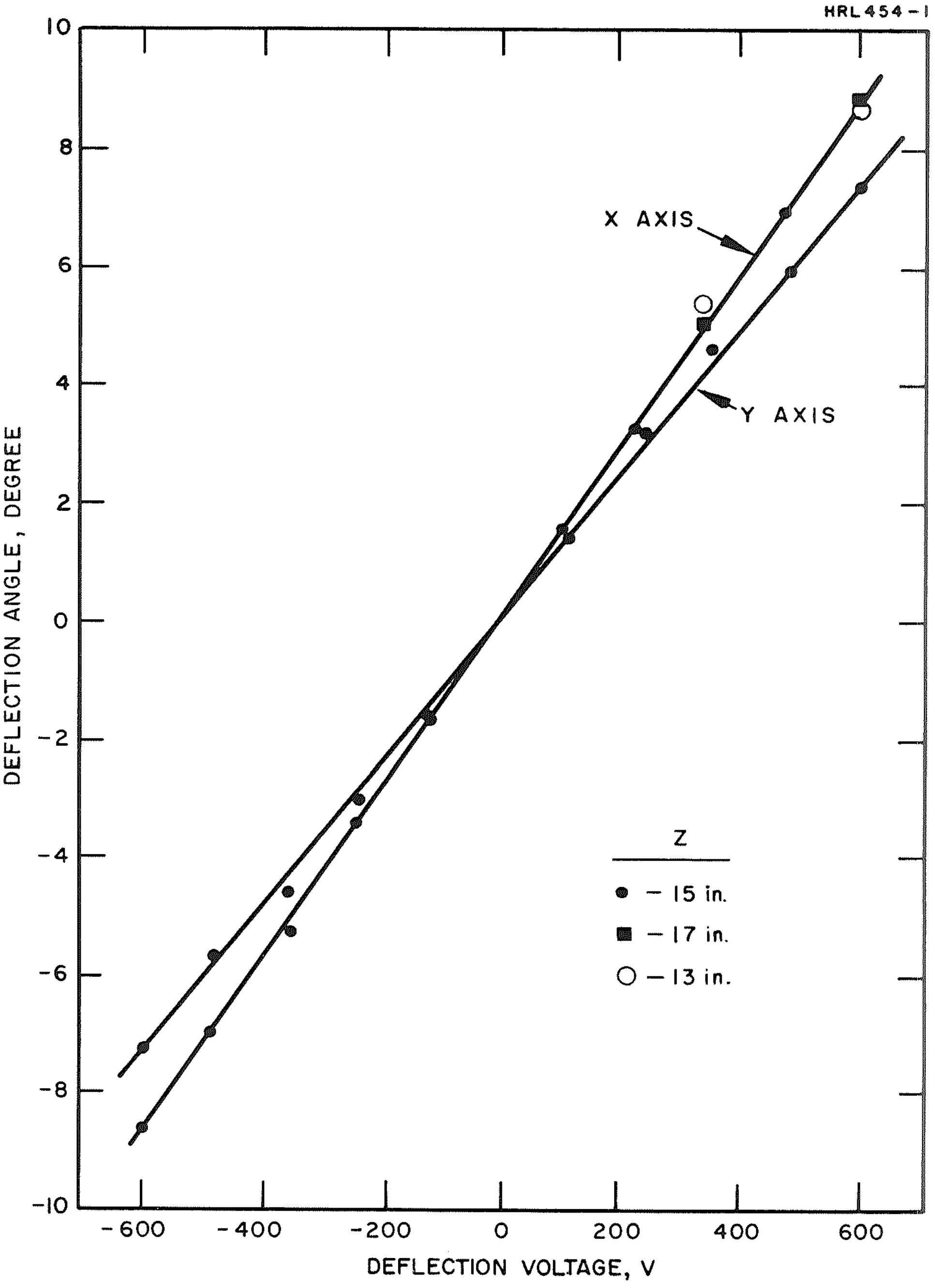

Fig. 27. X and Y Axis Deflection Sensitivities.

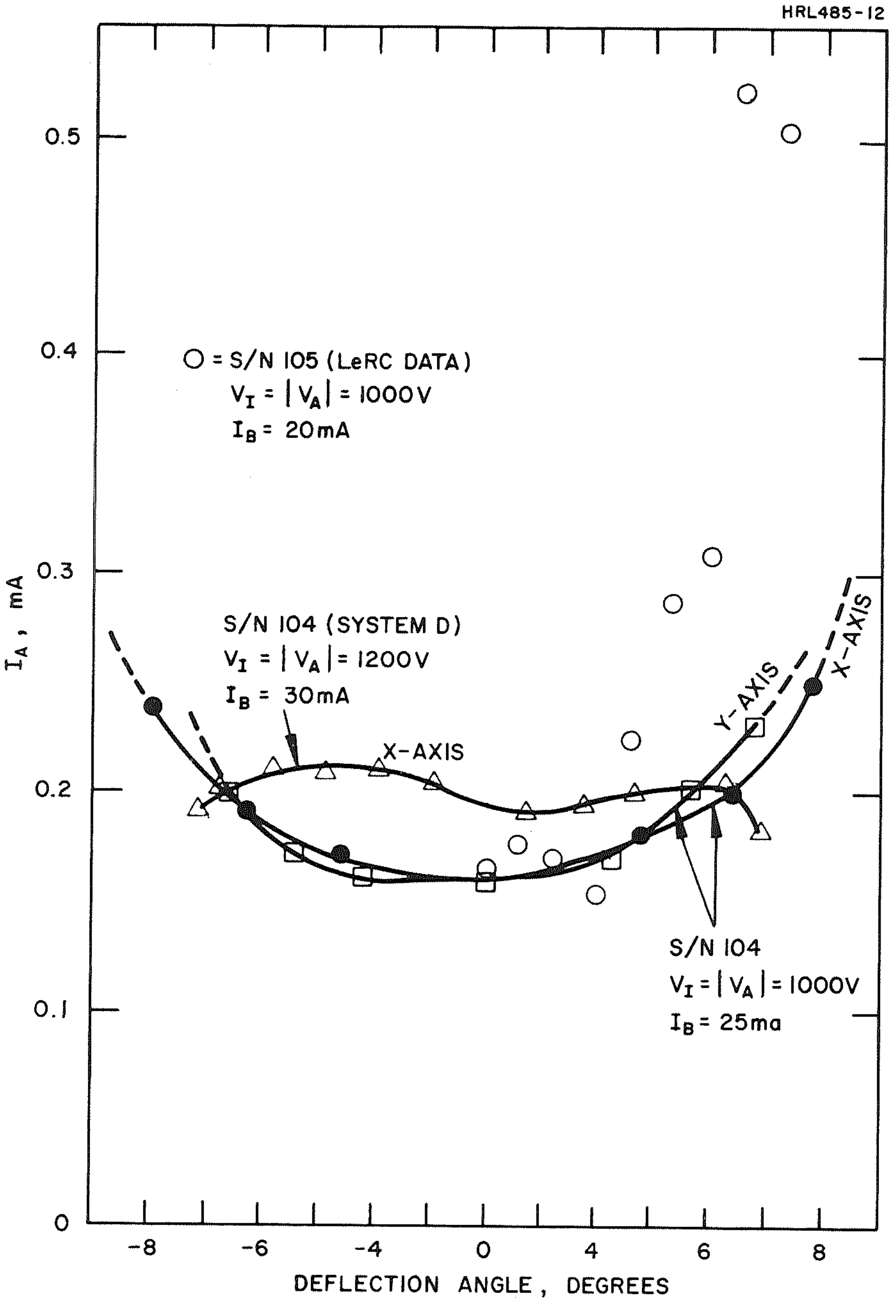

Fig. 28. Accelerator Current versus Deflection Angle for Dual Grid Electrostatic System.

current does not increase with increasing deflection angle and, in fact, at the higher angles the accel current appears to decrease. Establishing the true relationship between accel current and deflection angle was complicated by the fact that as the deflection angle was increased, the beam current would tend to decrease. The beam current was held constant by increasing the discharge voltage which should increase the mass utilization and plasma current density. One observable effect of increasing the discharge voltage was a decrease in accel current. Thus, small increases in accel current due to beam deflection could be offset by decreases caused when the discharge voltage was raised. For the data shown in Fig. 28, the discharge voltage and current varied from 36.5 V, 0.34 A to 37.5 V, 0.345 A when operating at an I_B of 25 mA and from 36 V, 0.42 A to 40 V, 0.45 A when operating at an I_B of 30 mA.

Due to the maximum differential voltage available from the deflection supply (700 V) the deflection angles obtainable with System D were limited to the values shown in Fig. 28. However, these results demonstrate that System D can operate at 30 mA I_B and satisfy the design objective of 10 degrees deflection without any significant increase in accel current.

Constant current density contours for Systems C and D are shown in Figs. 29 through 32. The almost octagonal shape of the undeflected contours for both these systems is a reflection of the screen electrode hole array. In the electrostatic system, the screen electrode hole pattern is square instead of the more conventional hexagonal pattern normally used to maximize the open area. The hole array is actually octagonal because the corner holes are eliminated to match the circular pole piece. This effect was made even more pronounced in System D by blocking off an additional two holes at each corner which had been partially obscured by the pole piece. Figure 29 shows both X and Y deflection contours for

System C. Figure 30 compares undeflected and equal angle X axis deflection contours for Systems C and D. The scans for System C were made without a neutralizer; those for System D were made with the plasma bridge neutralizer operating. Figure 31 presents contours for System D at three different deflections along the X axis. Figure 32 shows the contours that resulted when equal magnitude deflection voltages were applied in the plus and minus directions of the X and Y axes of System D. The distortions evident in Fig. 32 when deflecting in the +X and -Y directions are believed due to the presence of the neutralizer in the lower right corner.

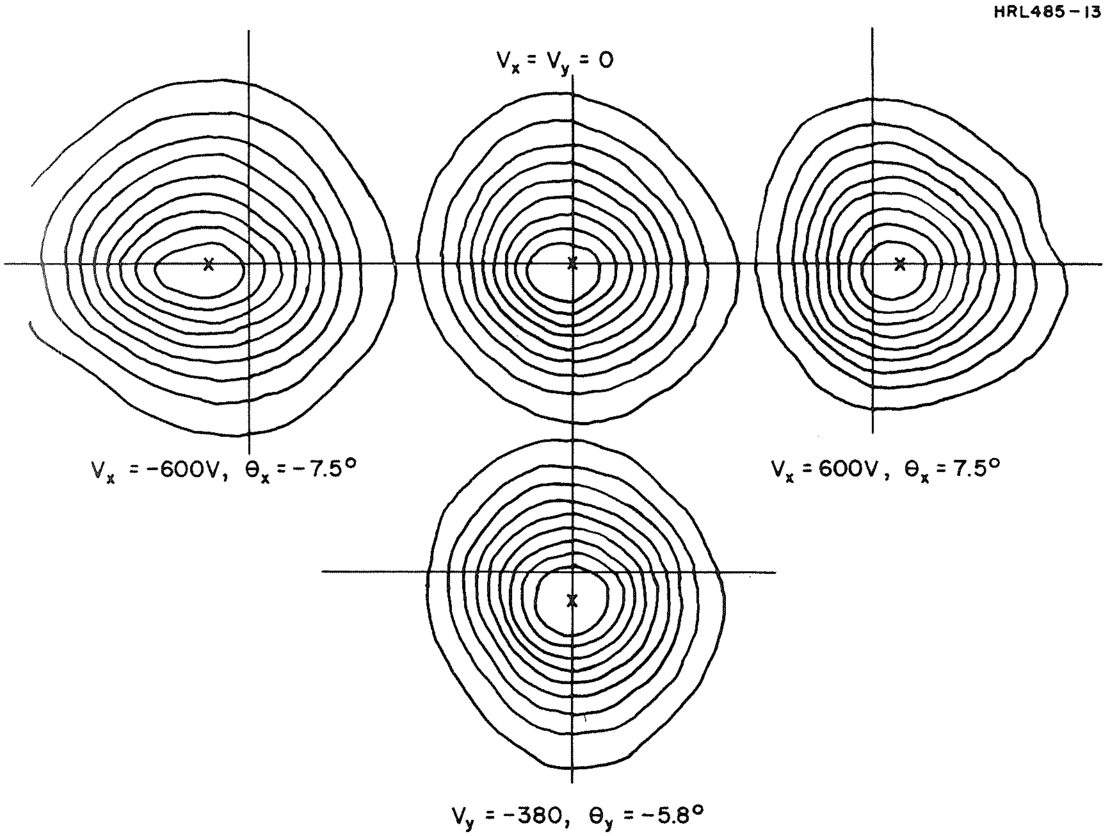

Fig. 29. Beam Profiles for Dual Grid Electrostatic System C under Several Operating Conditions.

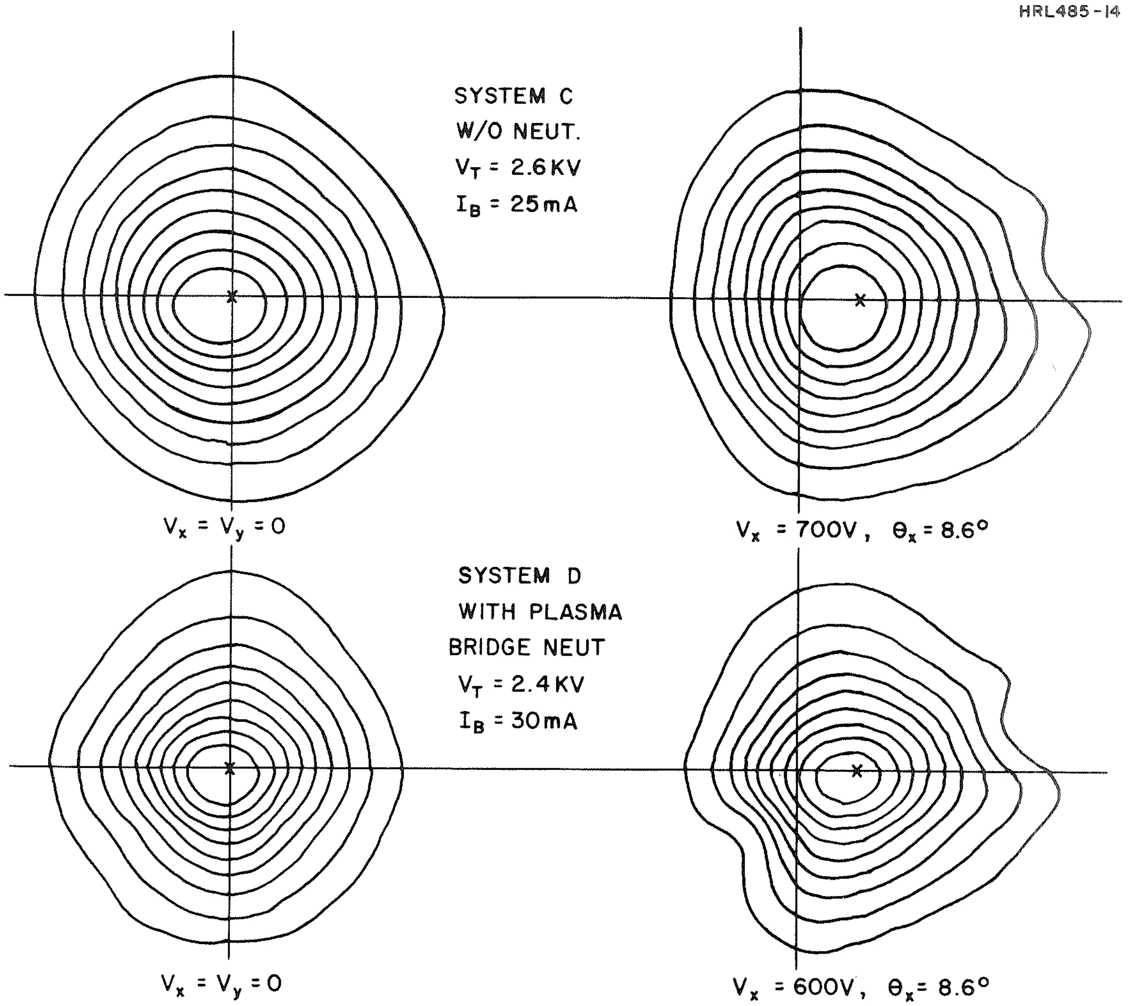

Fig. 30. Beam Profiles for Dual Grid Electrostatic Systems under Several Operating Conditions.

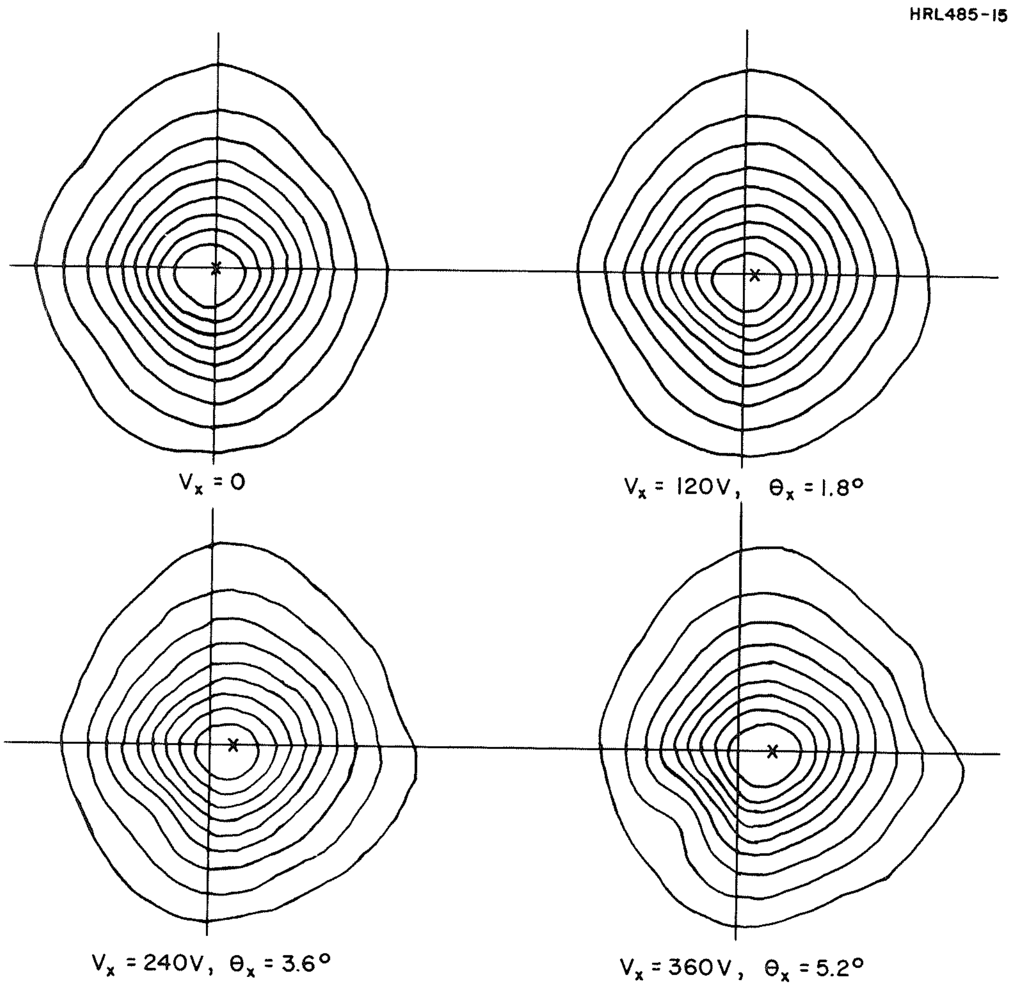

$V_x = 0$

$V_x = 120V, \ \theta_x = 1.8°$

$V_x = 240V, \ \theta_x = 3.6°$

$V_x = 360V, \ \theta_x = 5.2°$

Fig. 31. Beam Profiles for Dual Grid Electrostatic System D under Several Operating Conditions.

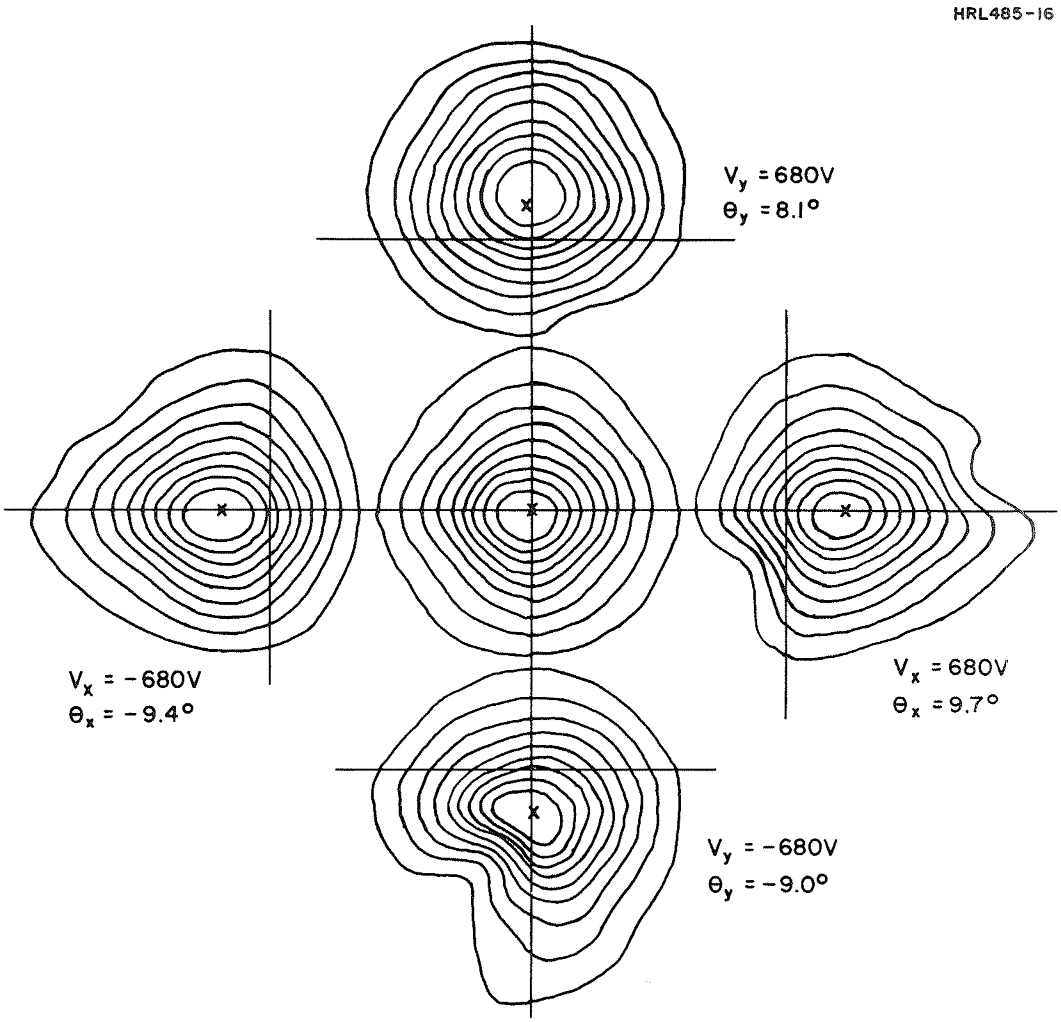

Fig. 32. Beam Profiles for Dual Grid Electrostatic System D under Several Operating Conditions.

B. ELECTROSTATIC SINGLE GRID SYSTEM

Testing of the single grid system was of only limited duration because of unsatisfactory performance. The accel current to beam current ratio was high (> 0.4) throughout the test. It was not possible to establish a condition of low accel current. The behavior of the thruster seemed to indicate that the insulating surface of the aluminum oxide coating was not acting as a screen grid. No deflection data were obtained because of the poor thruster performance. Since good deflection results had been obtained with both the movable screen electrode and dual grid electrostatic systems, further effort was not expended on the single grid electrostatic system.

C. MOVABLE SCREEN (APERTURE MISALIGNMENT SYSTEM)

Several mechanical configurations of this type of system were constructed and tested in order to achieve the desired performance in terms of:

- maximum deflection angle
- amount of electrode motion
- power required to obtain the specific deflection
- repeatability
- response time

All gave essentially the same performance in terms of deflection of the thrust vector for a particular electrode motion. Only the final configuration which was fully exercised is reported here. This unit had the dimensions shown in Table IV.

TABLE IV
MOVABLE SCREEN ELECTRODE CHARACTERISTICS

	Screen	Accelerator
Thickness, cm	0.063	0.127
Aperture diameter, cm	0.24	0.24
Aperture center-to-center spacing, cm	0.29	
Interelectrode spacing, cm	0.115	

T147

The electrode motion was measured by attaching the probe of a displacement transducer to the screen electrode. The response time and repeatability of screen electrode motion when deflecting and when returning to zero were determined by monitoring the output of this transducer. The repeatability was also confirmed by comparing the locations of the beam centroid as determined from the scanning beam probe measurements.

The movable electrode system was tested for a total of 32 hours before delivery to NASA LeRc. The maximum deflection angle measured was greater than 21 degrees. The design goal of 10 degrees was achieved with a deflection power of 1.1 W. (See Fig. 33.) The relationship between vertical deflection angle and screen translation is also shown in Fig. 33. (Screen motion was not measured in the horizontal axis because the weight of the transducer probe would have introduced a rotational force on the screen electrode.) With the thruster operating at 25 mA beam current and a total voltage of 2 kV the accel current remained less than 100 μA (0.4% drains) until the deflection angle exceeded 10 degrees. Accel current versus deflection angle is shown in Fig. 34.

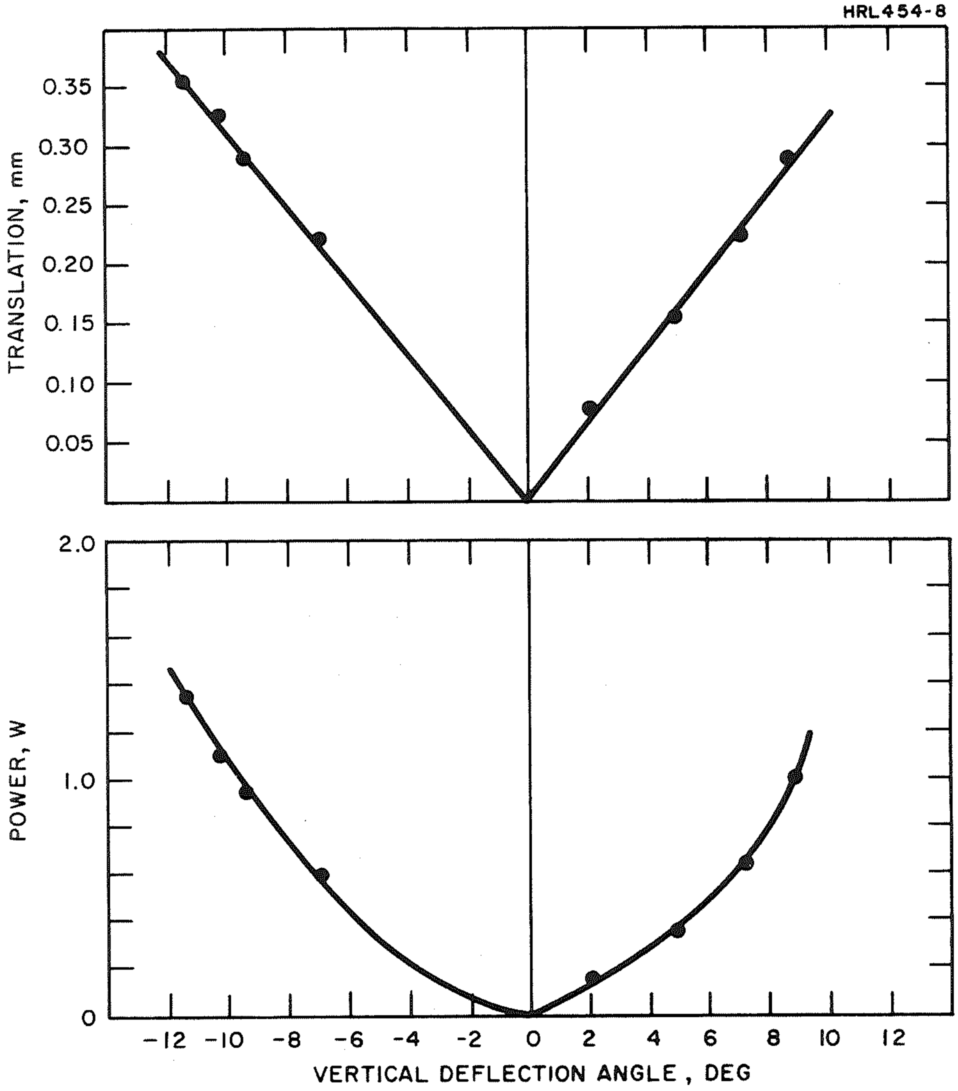

Fig. 33. Performance of Translating Screen Thrust Vector System.

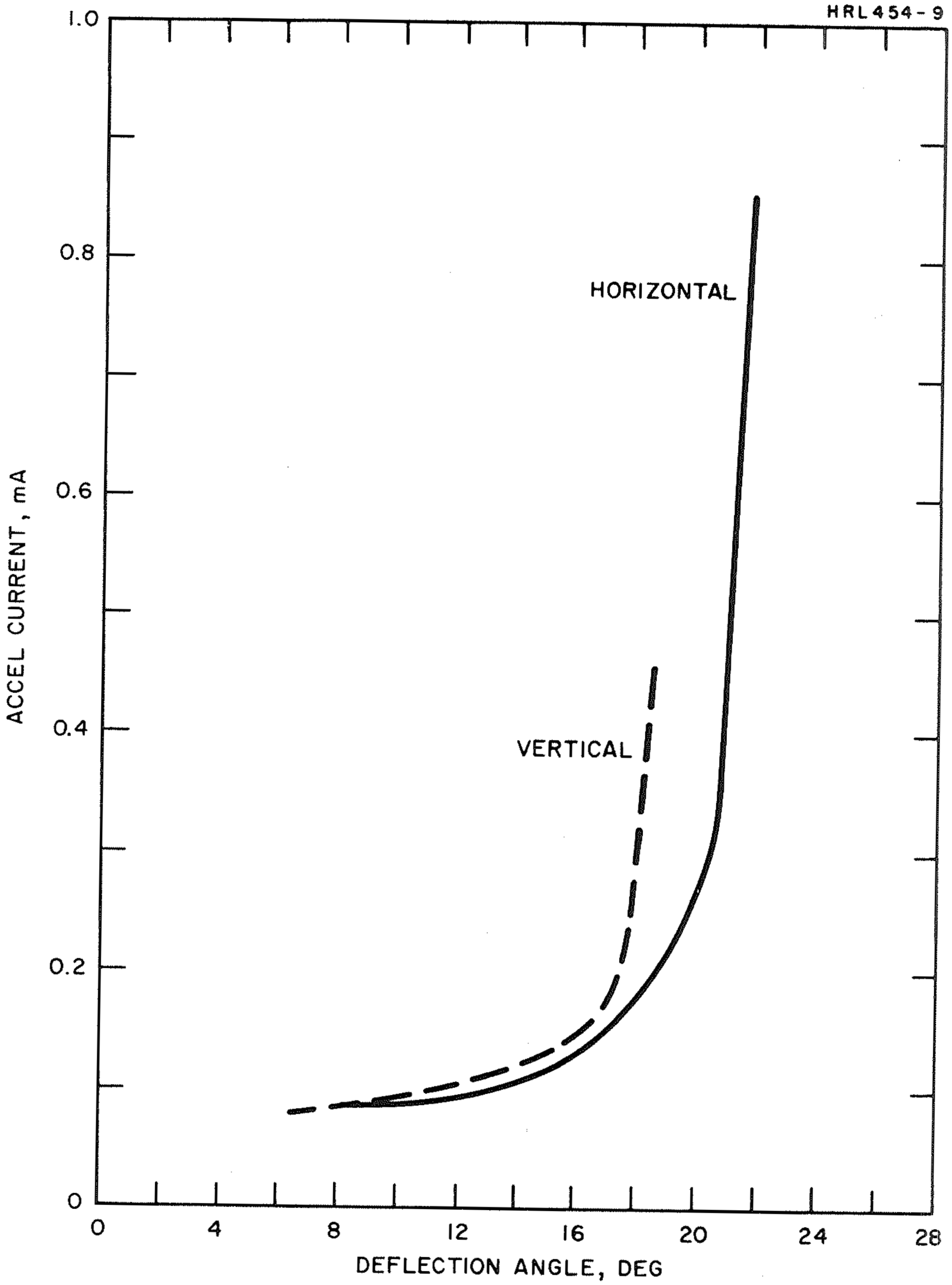

Fig. 34. Accelerator Current versus Deflection Angle for Translating Screen System.

The repeatability of the system was confirmed by the output of the displacement transducer and the location of the beam centroid. After 17 hours of testing which included seven vertical deflection cycles of up to 11.4 degrees (and five horizontal deflections) the displacement transducer output returned to its initial value when all deflection power was removed. The final zero deflection reading of the differential transformer after vertical deflections up to 18.4 degrees and horizontal deflections up to 21.8 degrees, indicated a shift in the electrode position of 0.014 mm (equivalent to approximately 0.5 degrees of deflection).

The response of the translating screen electrode system was relatively slow, when deflection was accomplished by applying only the amount of power required to achieve a given deflection, e.g., 10 min for 10 degrees deflection. Due to the long cooling time required, the time to return to zero after removing the deflection power was even longer, approximately 30 min to return from 10 degrees. The time to return to zero deflection from 10 degrees was shortened to one minute by heating the opposing springs to the same temperature and allowing both sets of springs to cool simultaneously. The return time could be reduced even further by applying the maximum safe power to the opposing springs and replacing the manual operation used in the experiment with electronic switching of a servo system. The time to displace the screen to a desired position of beam deflection can also be reduced appreciably by applying the maximum safe power until the desired position is reached, and then reducing the power to the amount required to maintain the spring temperature. This technique was used to reduce the deflection time from 10 min to 1 min.

The performance of the thruster when operating with the movable screen electrode deflection system is summarized in Table V. Note that the deflection sensitivity measured here

TABLE V

MOVABLE SCREEN ELECTRODE SYSTEM TEST RESULTS

A. DEFLECTION SYSTEM PERFORMANCE

1.	Deflection sensitivity	10 deg/0.031 cm of screen motion
2.	Power for 10 deg deflection	1.1 W
3.	Time to reach 10 deg deflection	
	Applying 1.1 W	∿ 10 min
	Applying 4 W	∿ 1 min
4.	Time to return to zero from 10 deg deflection	
	After removing power	∿ 30 min
	Applying 4 W to opposite springs	∿ 1 min
5.	No zero position error after deflecting to 10 deg	

B. THRUSTER PERFORMANCE

I_{beam} = 25 mA

I_{accel} = 0.08 mA (zero deflection)

V_{beam} = 1000 V

V_{accel} = 1000 V

eV/ion = 643 (in discharge)

η_{m_d} = 68.2% (without neutralizer)

T148

was 8 degrees for a motion of 0.024 cm, which is 10% of the screen aperture diameter. This compares well with the value of 8.4 degrees for a similar percentage motion predicted from the electrolytic tank studies.

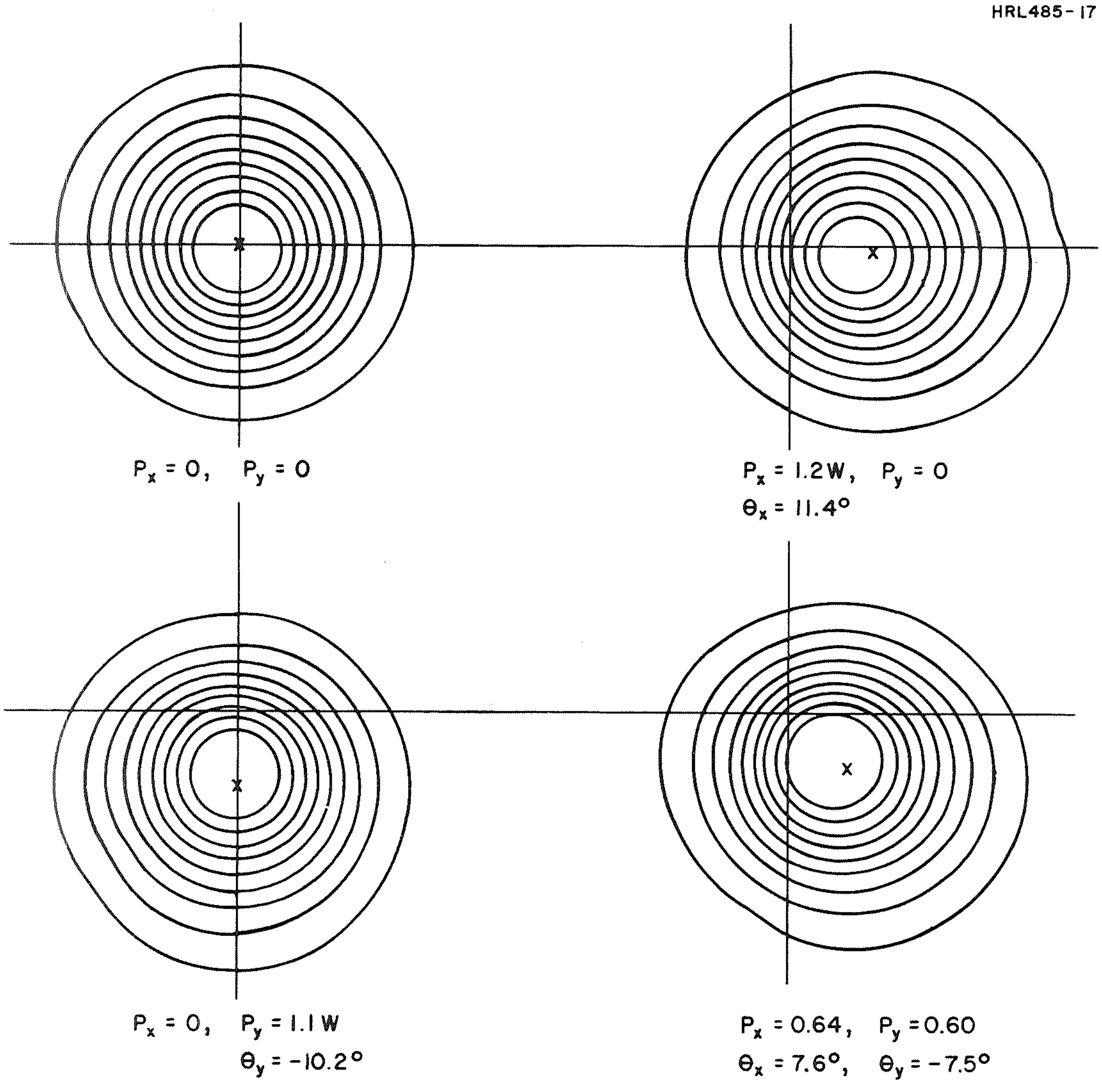

Fig. 35. Beam Contours for Movable Screen System.

In Fig. 35 constant current intensity contours for three conditions of deflection of the movable screen system* are shown: X axis deflection of 11.4 degrees, Y axis deflection of 10.2 degrees and deflection of 10.5 degrees at an angle of approximately 45 degrees between the X and Y axes. It can be seen that deflection out to the design goal of 10 degrees does not alter the shape of the contours significantly. Figure 36 shows the contours for the conditions of maximum deflection that were attempted with the movable screen system; 21.8 degrees in the X direction and -18.4 degrees in the Y direction. In Fig. 37, contours resulting from scans made at three different axial distances from the thruster are presented. The top two contours are for the same deflection condition taken at 38 and 25 centimeters, the bottom two contours show a second deflection condition taken at 38 and 50 cm. Contours such as these, taken at different distances from the thruster, provide a means of establishing the beam divergence. Figure 38 shows a plot of half-power beam radius versus distance downstream from the thruster for the movable screen electrode system. The beam divergence measured from these data is 13.2 degrees.

D. VECTORABLE DISCHARGE CHAMBER SYSTEM

The vectorable discharge chamber thruster mockup was bench tested in a vertical position to establish mechanical deflection characteristics. The deflection angle and azimuthal coordinates were measured by focusing the integral pinpoint light source on a coordinate chart placed 20 in. downstream on a plane normal to the thruster axis. The chart

---

*All movable screen data were taken without a neutralizer.

was aligned with the thruster axis while the stepper motors were in a neutral or zero-zero position. Power was applied in single pulse increments to each stepper motor in turn until each of the 144 possible deflection angles was plotted. These results are shown in Table VI.

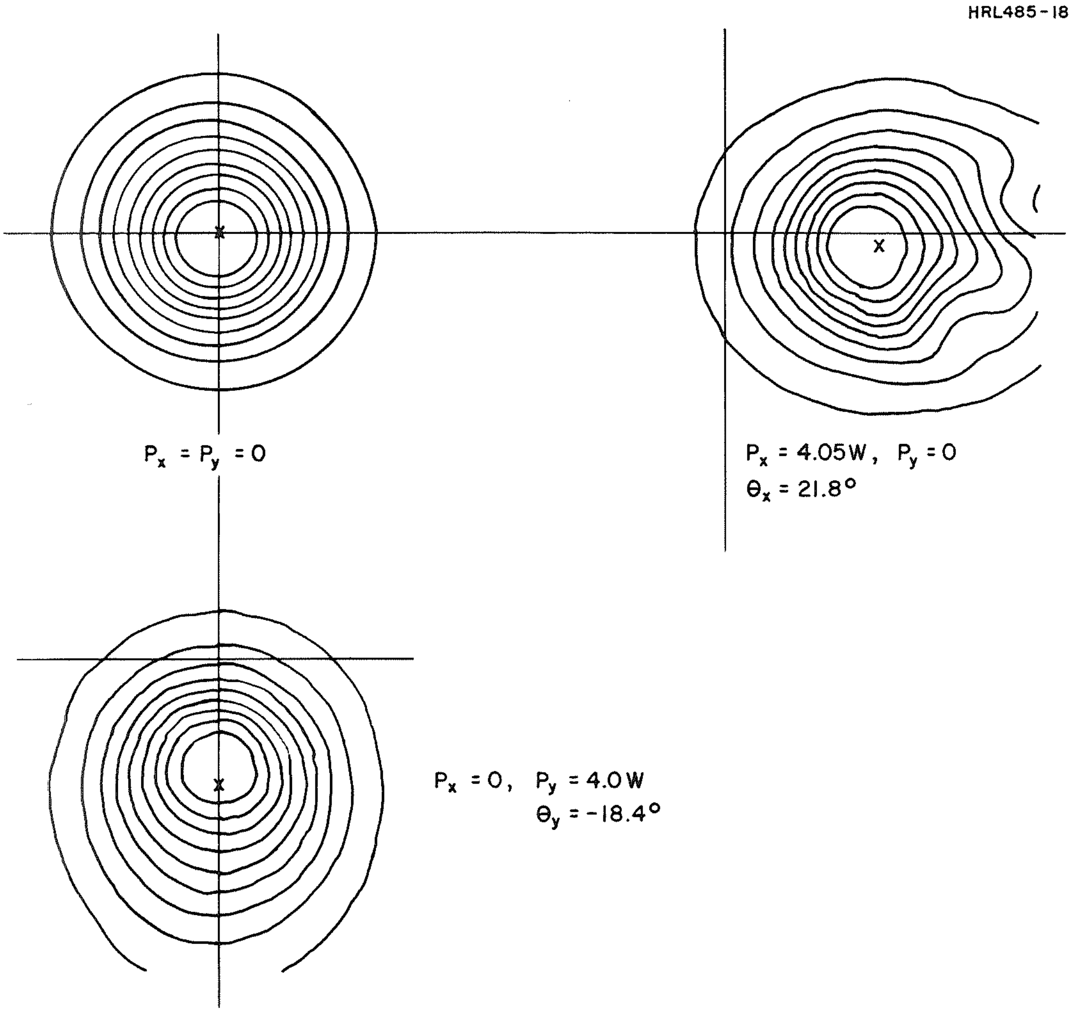

Fig. 36. Beam Contours at Maximum Deflection for Movable Screen System.

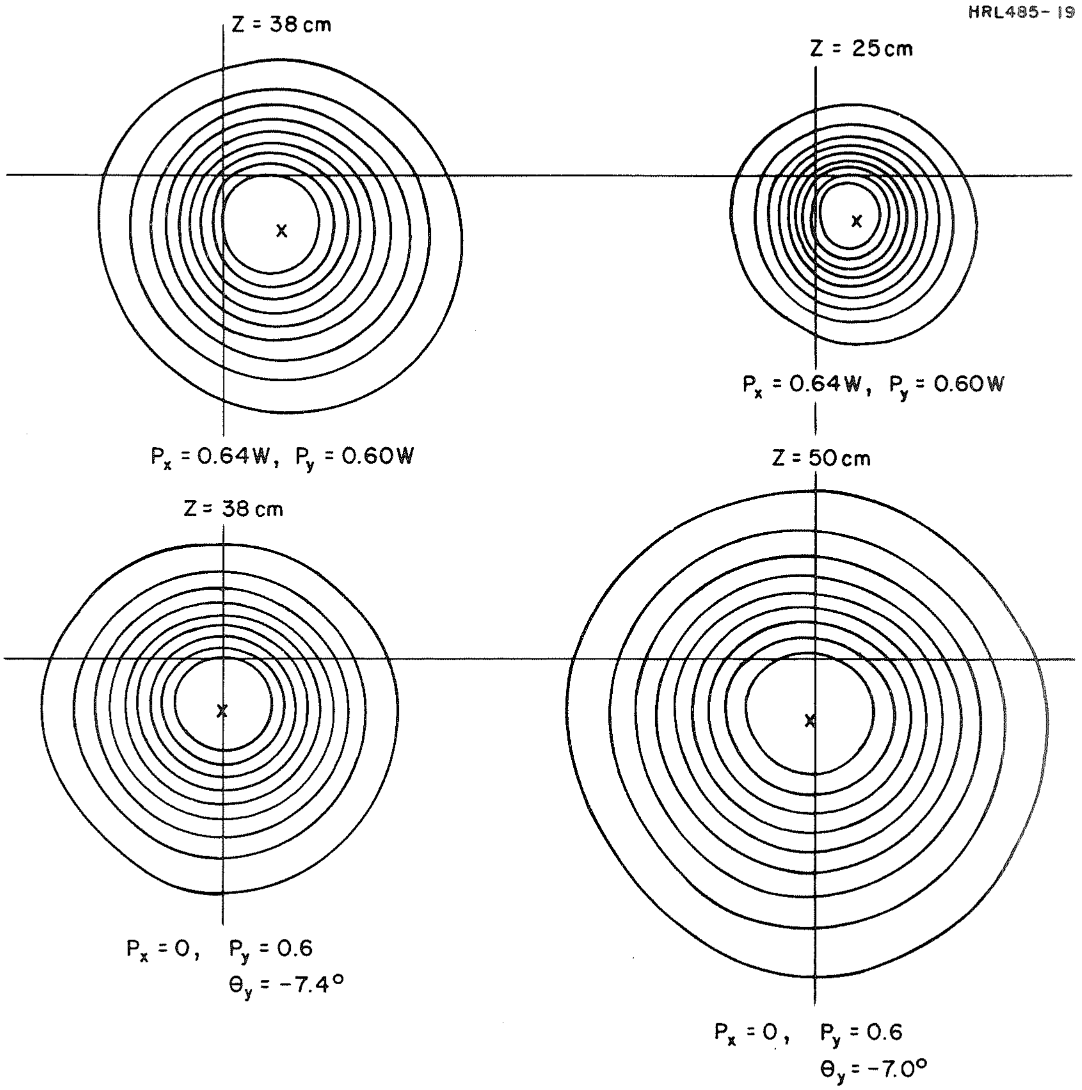

Fig. 37. Beam Contours at Three Z Distances.

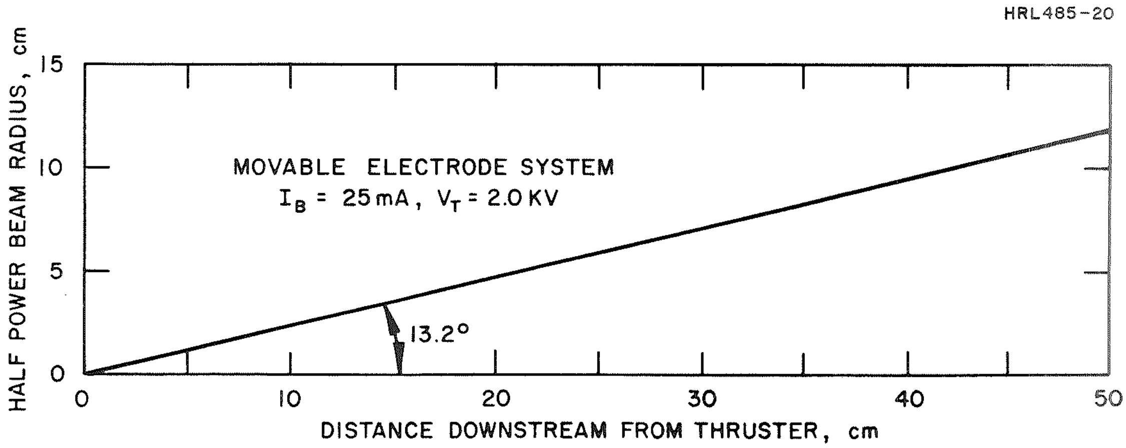

Fig. 38. Beam Radius versus Z Distance.

TABLE VI

BENCH TEST RESULTS OF VECTORABLE DISCHARGE CHAMBER THRUSTER MOCKUP

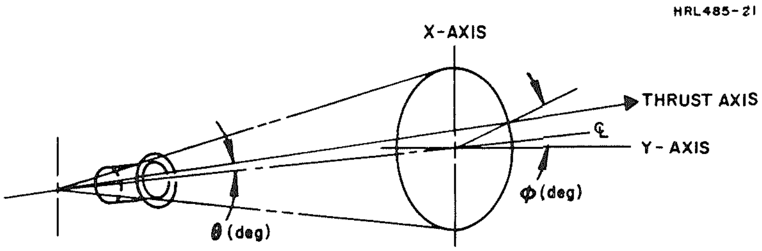

θ / φ KEY

		X AXIS NUMBER OF STEPS FROM ℄											
		0	1	2	3	4	5	6	7	8	9	10	11
Y AXIS NUMBER OF STEPS FROM ℄	0	0 0	5.8 270	10.0 270	11.1 270	9.4 270	5.1 270	0.8 90	7.0 90	11.9 90	13.6 90	12.0 90	6.2 90
	1	5.9 186	8.8 232	11.9 240	13.0 243	11.1 237	7.9 220	5.9 170	9.0 128	12.9 115	14.0 112	12.5 115	8.0 135
	2	10.5 187	12.6 214	15.0 225	15.5 227	14.0 222	11.5 205	10.5 173	12.6 145	15.2 132	16.0 129	15.0 133	11.7 153
	3	12.6 187	14.1 210	16.0 221	16.5 272	15.5 217	13.5 200	12.8 174	14.7 150	17.0 137	18.0 135	16.5 140	13.6 158
	4	11.9 186	13.5 212	15.4 223	16.0 236	14.8 220	12.8 202	12.2 173	14.4 150	17.0 137	18.0 135	16.4 140	13.2 157
	5	8.4 187	6.2 221	12.9 235	13.8 238	12.0 232	9.5 210	9.0 171	11.9 142	15.0 130	12.8 128	14.2 132	10.4 132
	6	3.2 190	6.9 248	10.5 260	11.7 262	9.8 257	5.7 240	3.8 163	8.3 121	12.4 112	13.9 110	12.0 112	6.9 126
	7	2.1 3	6.2 298	10.3 290	11.8 288	10.1 290	5.9 298	2.1 50	6.6 77	11.5 85	13.0 87	11.5 85	6.8 78
	8	7.0 10	9.0 328	12.2 313	13.8 308	12.8 312	9.2 325	7.0 2	9.0 45	13.1 63	15.0 67	13.8 64	9.8 50
	9	9.6 11	10.8 337	13.6 321	15.0 316	14.3 318	11.2 334	10.0 2	11.5 37	15.0 54	16.5 57	15.5 56	12.0 45
	10	9.0 14	9.9 335	12.8 318	14.0 313	13.3 315	10.3 331	9.1 5	11.0 40	15.0 55	16.5 58	15.5 57	12.0 45
	11	6.3 17	7.5 325	10.8 307	12.2 302	11.2 305	8.0 321	6.1 8	9.5 50	13.9 63	16.0 65	14.5 64	10.0 53

T149

SECTION VI

SYSTEMS COMPARISON

Table VII compares the three types of thrust vectoring systems on the basis of the criteria set forth in Table I, Section III. On the basis of this evaluation, the electrostatic dual grid system was chosen for further development in the 5 cm size and for the 100 hour endurance test that is reported in the following section. Speed of response and absence of any moving parts were considered particularly critical factors in this decision.

The performance of the LeRC 5 cm thruster when operating with the dual grid electrostatic system, moving screen electrode system, and a single glass coated nondeflectable optic is presented in Table VIII.

TABLE VII

COMPARISON OF THRUST VECTORING SYSTEMS

CRITERION	TYPE OF SYSTEM		
	DUAL GRID ELECTROSTATIC	MOVABLE SCREEN ELECTRODE	VECTORABLE DISCHARGE CHAMBER
Deflection Angle	Continuous deflection to greater than 10 deg	Continuous deflection to greater than 15 deg	Discrete deflection angles to 10 deg (continuous with modified design)
Deflection Azimuth	Continuous deflection to any azimuth	Continuous deflection to any azimuth	Deflection to discrete azimuths
Response Time	Electrical, $< 10^{-4}$ sec	Thermal, 10 to 100 sec	Mechanical ~ 1 sec
Pointing Accuracy	High accuracy with closed loop control	High accuracy with closed loop control	Better than 1 deg (may change with time)
Lifetime	Little accel erosion at $\theta < 10$ deg. Interelectrode insulators susceptible to sputter deposition.	Little accel erosion at $\theta < 15$ deg	Approximately equal to a non-vectorable system
Thruster Performance	Discharge eV/ion increased	Discharge eV/ion increased	No effect
Adaptability	Tested on 5 cm thruster, mechanically difficult for 30 cm thruster	Adaptable to both 5 and 30 cm thrusters	Adaptable to 5 cm thruster; More difficult for 30 cm thruster
Tested Concept	Tested on 5 cm for 100 hours. No satisfactory design for 30 cm to date	Tested on 5 cm, mockup demonstrated for 30 cm	Tested on 5 cm mockup
Development Time and Cost	5 cm prototype design ready for qualification — 30 cm difficult	5 cm demonstrated — 30 cm prototype design ready at end of this contract	Prototype demonstrated for 5 cm thruster
Weight	Present 5 cm design Total grid weight = 210 g Added system weight = 3.9%	Present 5 cm grid design Total grid weight = 305 g Added system weight = 5.1%	Added system weight ~ 500 g ($\sim 21\%$)
Power	Less than 1 W at $\theta = 10$ deg	Approximately 1 W at $\theta = 10$ deg	50 W, 50 msec pulse to actuate; steady-state - none
Reliability	No moving parts - possible failure mode - by accel erosion or insulator leakage	Spring and flexure deflection only motion required - no additional high voltage insulators	Mechanical actuators required
Power Conditioning Required	Two ~ 1 kV power supplies required - Closed loop control desirable	Two low voltage heater supplies required - Closed loop control desirable	Two pulse supplies required - Open loop control adequate
Thruster Design	No change in discharge chamber Minimal structural change	No change in discharge chamber Minimal structural change	No change in discharge chamber Modified mounting required

T150

TABLE VIII

5 cm THRUSTER PERFORMANCE WITH THREE OPTICS SYSTEMS

Parameter	Optics System		
	Dual Grid Electrostatic Deflection	Movable Screen Electrode Deflection	Single Grid Glass Coated (Nondeflecting)
V_{beam}, V	1200	1000	600
I_{beam}, mA	30	25	36
V_{accel}, V	1200	1000	410
I_{accel}, mA	0.2	0.08	0.2
$V_{discharge}$, V	37.1	38.1	37.1
$I_{discharge}$, A	0.43	0.42	0.26
Specific Impulse, sec	2240	2160	1670
Thrust, mlb	0.48	0.36	0.44
eV/ion	528	643	268
η^*_m discharge, %	64.5	68.2	68.0
$\eta^*_{electrical}$, %	48.2	39.0	41.3

*These efficiencies do not include the electrical power or mass flow of the neutralizer.

T152

SECTION VII

ENDURANCE TEST OF DUAL GRID ELECTROSTATIC DEFLECTION SYSTEM

A. INTRODUCTION

The preceding section compares the performance of the four most promising deflection systems studied under this program. Most of the data was collected in relatively short (i.e., 5 to 10 hour) tests. In order to demonstrate the stability of the system and to provide an experimental basis for estimating the minimum useful lifetime, a 100 hour endurance test was conducted as the final phase of the test program. Based on the results of the preceding section, either the dual grid electrostatic or translating screen electrode systems could have been used for this test. After consultation with the NASA Program Manager, the electrostatic system was chosen. A new optic set was fabricated and the test begun, using the same test facility as for the shorter tests.

B. 100 HOUR TEST

The 100 hour test was completed without any observable changes in deflection system sensitivity or thruster performance. Slight erosion was visible on a few of the y-axis deflection electrodes at the conclusion of the test. During the 68th hour of the test, a temporary short was detected between the top and right deflection electrodes. Due to deposition of sputtered material on the interelectrode ceramic spacers, the interelectrode current for 480 V deflection voltage was 1.5 mA at the end of the test.

C. TEST PROCEDURE

The test plan approved for this test was as follows.

- Operate the thruster at a beam current of 30 mA, a net accelerating voltage of 1200 V (V_I), and a total accelerating voltage of 2400 V (i.e., $V_A = -1200$ V).
- Collect deflection data by making a two-axis scan with the beam probe according to the following schedule.
    - At the beginning and end of the test deflect in approximately 2 degree intervals up to 10 degrees (or the voltage limit of the deflection supply) along the +X, -X, +Y, and -Y axes in one plane. In two other planes (different z distances) scan at zero deflection and full deflection in one direction.
    - Every twelve hours measure the deflected beam in approximately 2 degree intervals up to 10 degrees along the + X axis and at 10 degree deflection along the -X, +Y, and -Y axes.

D. TEST RESULTS

The consistency of the deflection system is illustrated by the deflection results from the measurements made at the beginning and end of the test which are plotted in Fig. 39 (X-axis) and Fig. 40 (Y-axis). The X-axis deflection angle versus deflection voltage results at the end of the test had an offset from zero of approximately 1.2 degrees. This was caused by a shift in the reference voltage applied to the potentiometer from which the X position of the probe is obtained. This voltage change was detected during the final set of deflection measurements and corrected. However, the error existed at the time the undeflected beam scan was made,

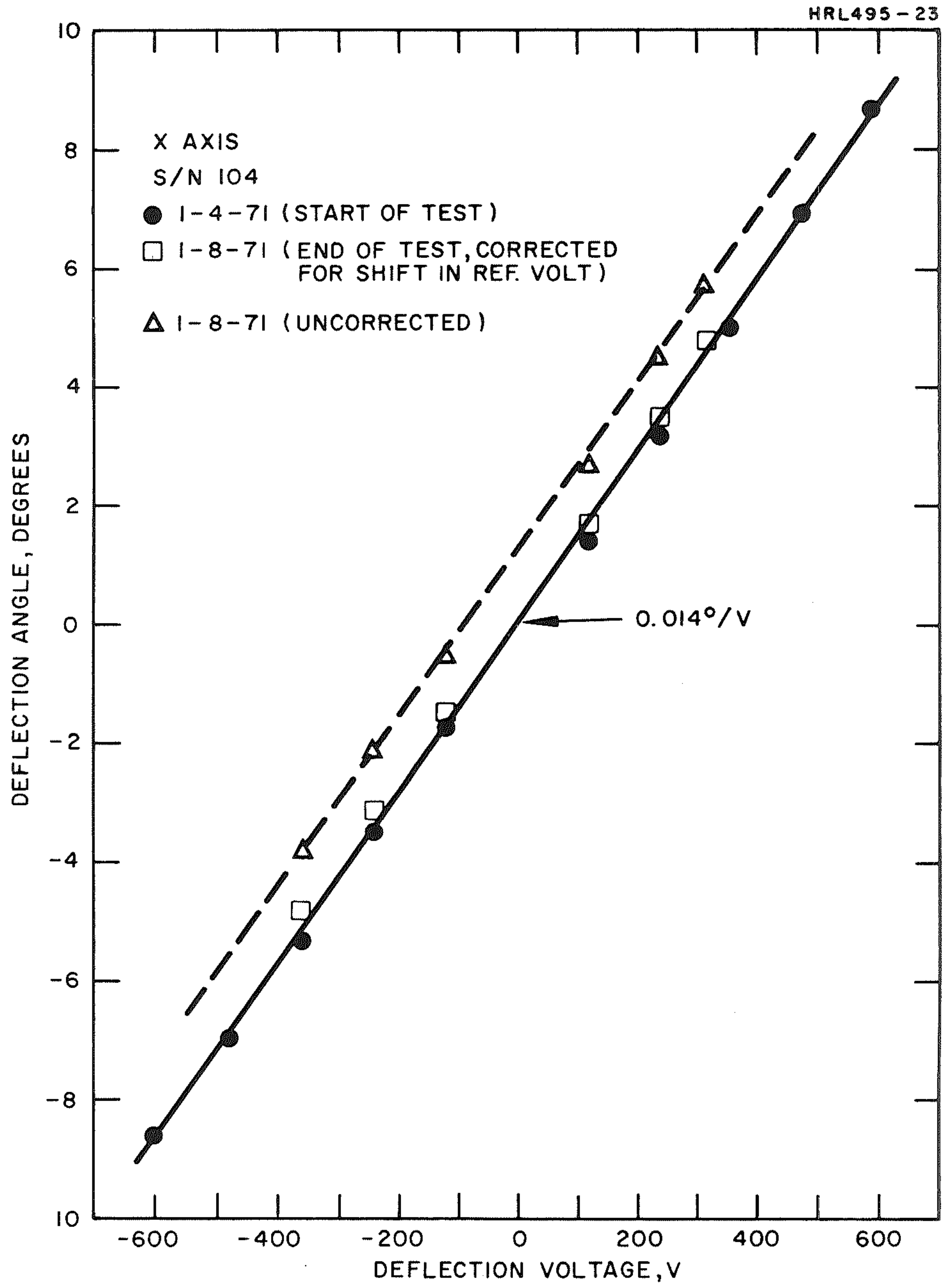

Fig. 39. X-Axis Deflection Angles Measured at Beginning and End of 100 Hour Test.

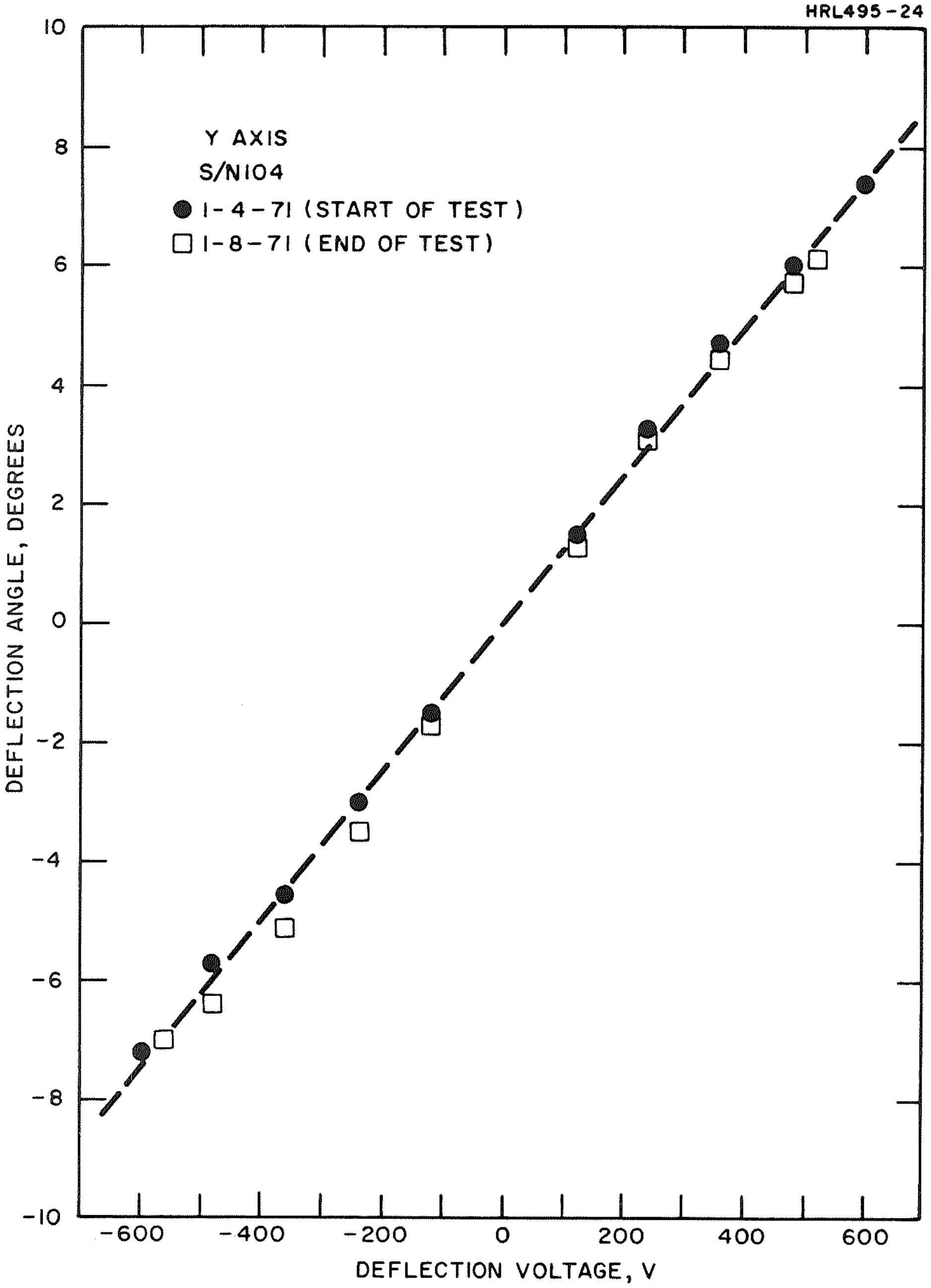

Fig. 40. Y-Axis Deflection Angles Measured at Beginning and End of 100 Hour Test.

and therefore the location of the X coordinate of the undeflected beam was affected. The corrected data points for 1-8-71 shown in Fig. 39 were obtained by using the X coordinate for the undeflected condition on 1-6-71. It is important to note that though the uncorrected X-axis results at the end of the test did have an offset due to the reference voltage change, the deflection sensitivity had not changed from the measurements made at the beginning of the test. The most deflection data were obtained for the positive X-axis. The results of averaging all the measurements made along the +X axis are presented in Fig. 41. The angles measured at three different Z distances (33, 38, and 43 cm) agreed within 10%.

The test plan was followed without incident until the first deflection measurement on the fourth day of the test (during the 68th hour), when it was discovered that a short existed between the top and right deflection electrodes. While this short remained, X-axis deflection measurements were made with the top, bottom, and right electrodes connected together externally. The deflection angles measured under these conditions were similar to the angles measured prior to the short. During the next scanning period (74th hour), it was found that the electrodes were no longer shorted. The remaining deflection measurements were made in the normal manner.

As the test proceeded, the leakage current between the deflection electrodes increased due to sputtered material depositing on the ceramic spacing disks between electrodes. By the end of the test, the overcurrent trip circuits in the deflection supply would trigger when trying to apply the full 600 V deflection voltage. It was noted that though the dc trip level of the supply is between 3.5 and 4.5 mA, due to transients the supply always tripped off before the current

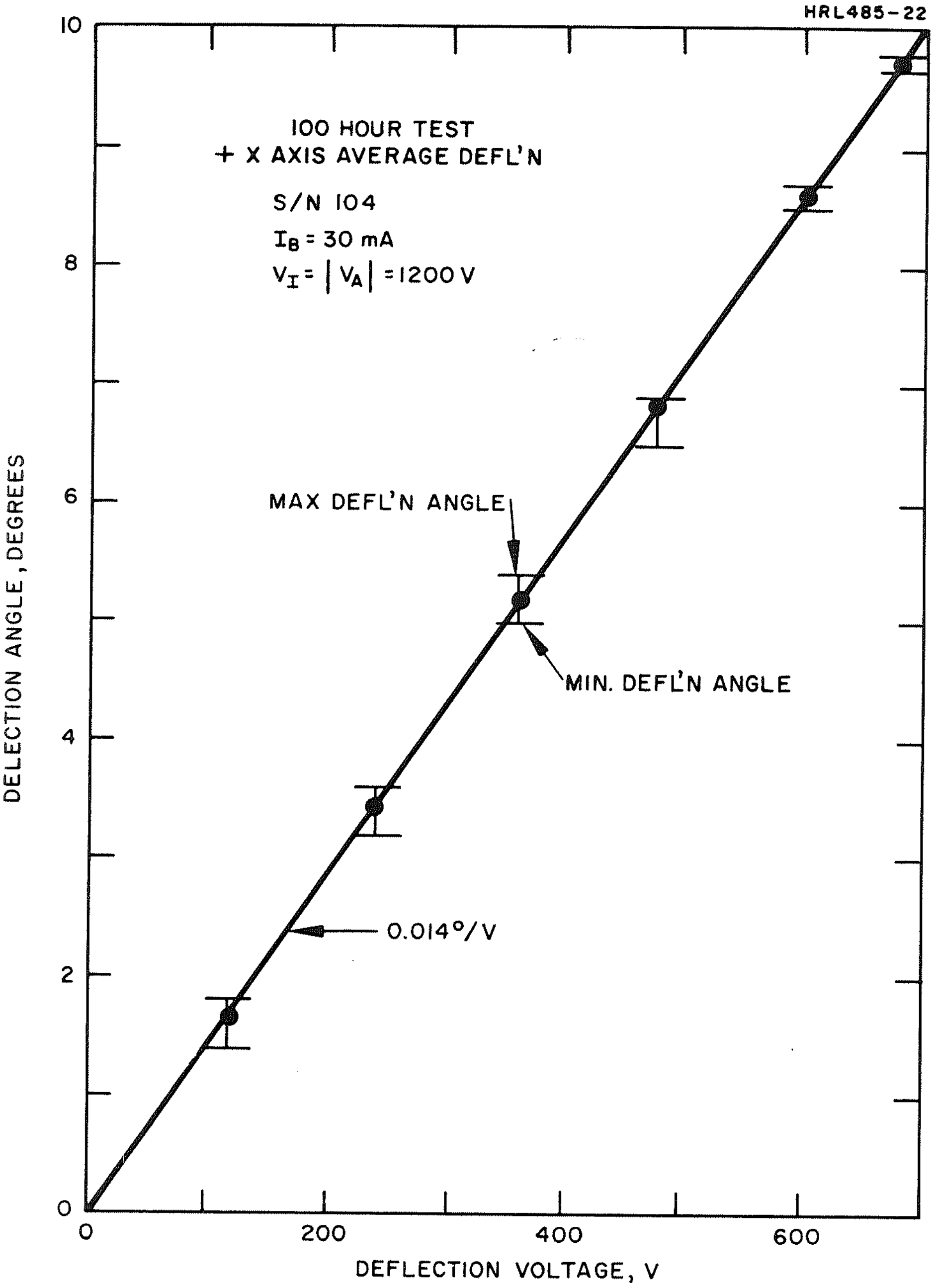

Fig. 41. Average Positive X-Axis Deflection Angles Measured During 100 Hour Test.

meters even reached 3 mA. At the completion of the test after making as many of the scheduled deflection measurements as possible with the above deflection supply, an attempt was made to apply full deflection voltage with a higher current capacity supply. With this supply connected between the X-axis deflection electrodes, an attempt to apply 600 V caused a short to develop between the top and right deflection electrodes.

The performance of the thruster throughout the test was very stable. The only deviations from normal operation were when the plasma bridge neutralizer keeper went out, once during the 47th hour and once again during the 57th hour. The thruster was also turned off for 2 hours after the temporary short between electrodes was discovered and then restarted without any difficulty. The performance of the deflection system and thruster is summarized in Table IX.

TABLE IX

100 HOUR TEST PERFORMANCE SUMMARY

DEFLECTION SYSTEM PERFORMANCE	
Deflection Sensitivity	0.014 deg/V X-axis
	0.012 deg/V Y-axis
Interelectrode Current (for deflection voltage of 480 V)	<0.10 mA at start 1.5 mA at end
THRUSTER PERFORMANCE	
I_{beam}	30 mA
I_{accel}	0.21 mA
V_{beam}	1200 V
V_{accel}	1200 V
$V_{discharge}$	37.1 V
$I_{discharge}$	0.427 A
eV/ion	528
η_m (discharge only)	64.5%

T153

E. POST TEST ANALYSIS

The appearance of the deflection system (and thruster) following the 100 hour test was very good. The condition of the individual deflection electrodes is shown in Figs. 42(a) and (b). Some slight erosion occurred on the stiffening ribs of a few of the Y-axis deflection electrodes. The direct short between electrodes that had occurred at the conclusion of the test when a higher power supply was substituted for the deflection supply disappeared before the system could be examined outside the test chamber. It is believed that these temporary shorts were caused by movement of the electrodes due to thermal expansion from the interelectrode current. This possibility has been eliminated in the most recent design where the individual electrodes are held in position under spring tension.

The source of the decrease in impedance between electrodes which caused the interelectrode current was obvious when the deflection system was disassembled. The ceramic spacers between adjacent electrodes had become lightly coated with sputtered material. This problem also will be alleviated by the most recent design in which the disk spacers are replaced by a ceramic bar which is positioned well upstream of the accelerator plane and can be more effectively shielded.

F. CONCLUSIONS

The deflection characteristics of this dual grid electrostatic deflection system remained unchanged throughout the 100 hour test. Two problem areas were identified as a result of the 100 hour test: (1) a buildup of interelectrode current due to sputter deposition on the ceramic disk interelectrode spacers and (2) interelectrode shorting due to thermal expansion of the electrodes caused by the interelectrode current. Both of these problems should be eliminated by the most recent design of the dual grid electrostatic deflection system.

M 7681

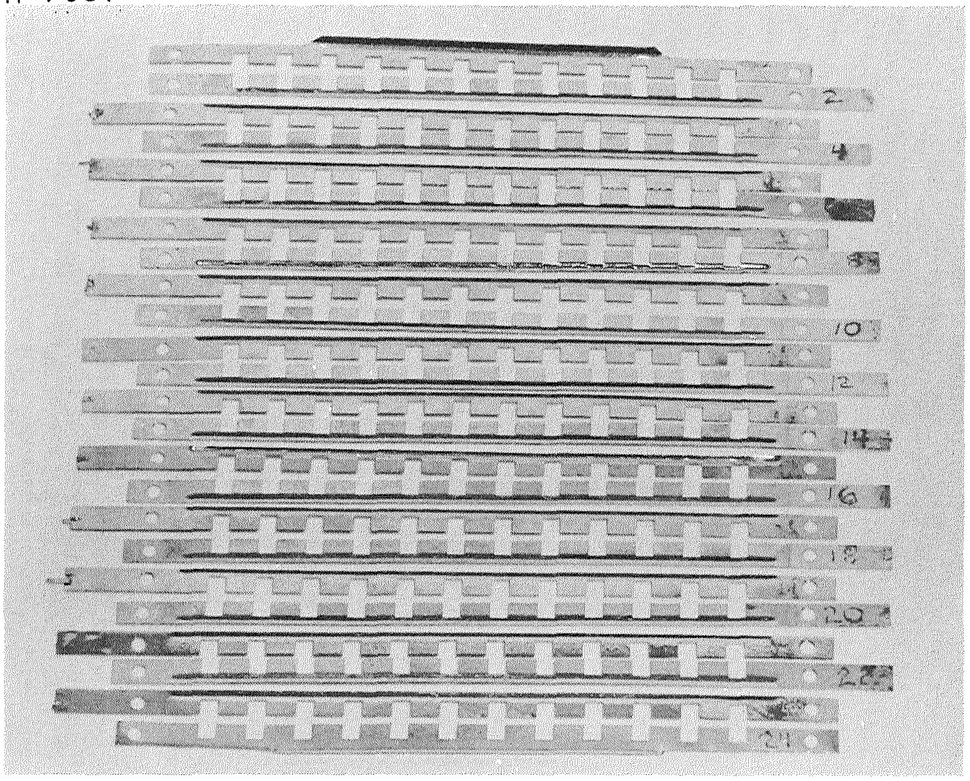

(a) X Axis.

Fig. 42. Deflection Electrodes after 100 Hour Test.

M 7680

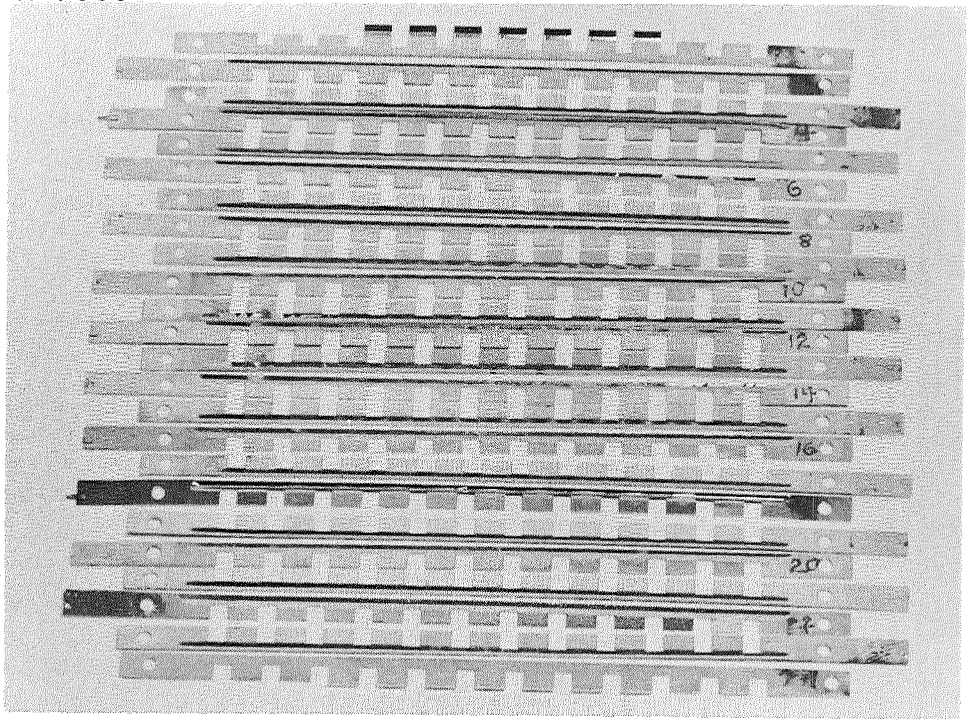

Fig. 42(b). Y Axis.

SECTION VIII

DELIVERABLE HARDWARE

In fulfillment of the hardware delivery requirements of this program, the following deliveries were made: three dual grid electrostatic systems (grid assembly S/N 102, 105, and 106) as shown in Fig. 7; one single grid electrostatic system (S/N 103) as shown in Fig. 8; one movable screen electrode system as shown in Fig. 14; one vectorable discharge chamber thruster mockup as shown in Fig. 15.

SECTION IX

CONCLUSIONS

The goals of the effort reported here were to first make a survey of the various conceptual means of vectoring the beam from a mercury bombardment ion thruster, second, to select the best of these systems based on analytical models and preliminary experiments, third to fabricate hardware representative of at least three systems and to experimentally evaluate each of these designs and finally to select the most promising of the systems and endurance test it for 100 hours. On the basis of the above sequence four systems were fabricated. These were the dual grid electrostatic, the single grid electrostatic, the movable screen electrode, and the vectorable discharge chamber. Of these only the single grid electrostatic (which had been considered speculative from its inception) did not meet specifications. Of the other three, the dual grid electrostatic was considered most promising for the intended application due to its high response speed and the absence of any moving parts. Although slower, the movable screen electrode is more easily adaptable to larger thrusters and was able to provide deflection angles up to 15 degrees as compared to 10 degrees for the electrostatic system without direct interception. The vectorable discharge chamber had the advantage of not modifying the thruster performance in any manner but was rated third because of the mechanical actuator, and the fact that control of the beam direction was in discrete steps rather than being continuous. An extensive comparison of the characteristics of the three systems has been presented in Table VII.

In summary, it has been shown that the ion beam from a 5 cm thruster (and hence the thrust direction) can be continuously vectored to greater than 10 degrees by both electrical and mechanical means. Furthermore, it has been illustrated that the performance of both types of systems can be predicted on the basis of analytical models derived from a basic knowledge of ion optical systems and a computer simulation of space charge limited flow. These basic models and the construction techniques demonstrated in this program can serve as the basis for future development of both 5 cm and larger thrust vectoring systems.

REFERENCES

1. "Vectorable Ion Optical Systems," Preliminary Report submitted under Contract NAS3-14058, HRL Staff, May 1970.

2. "Design of Electrostatic and Mechanical Thrust Vectoring Systems," submitted under Contract NAS 3-14058, HRL Staff, July 1970.

3. J.R. Anderson and G.A. Work, "Ion Beam Deflection for Thrust Vector Control," J. Spacecraft and Rockets, 3, 1772 (1966).

4. R.M. Worlock, *et al.*, "Cesium Bombardment Ion Engine System", Technical Report AFAPL-TR-69-87 (1969).

5. K.R. Spangenberg, *Vacuum Tubes*, McGraw-Hill, 1948.

6. "Ion Engine Thrust Vector Study," Final Report, Contract JPL 952129, 1970, HRL Staff.

7. W. Lathem, "Effect of Misalignments in Kaufman Thrusters," J. of Spacecraft and Rockets 5, 735 (1968).

8. S. Timoshenko and D. Young, *Strength of Materials*, 4th Edition, 1961.